Chapter 9—A Quantum Chemistry Explanation of the Alkoxy Relative Kinetics “Low [O_2] Anomaly”

Abstract

In Chapter 7, we observed that the primary products of alkoxy isomerization, HOR• (absence of O_2) and HOROO• (presence of O_2), have ν_1 (OH stretch) bands with different peak shapes and intensities. We used these peaks to measure the relative kinetics of alkoxy isomerization to reaction with O_2 ($k_{\mathrm{isom}}/k_{\mathrm{O2}}$) in Chapter 8 by measuring the relative absorbance A_0/A vs [O_2]. This relationship is expected to be approximately linear, with A_0/A increasing with O_2. However, for very low [O_2] ($0 < [O_2] < 3 \times 10^{16}$ molec cm^{-3}), we observe anomalous behavior: A_0/A is not equal to 1 at [O_2] = 0, and A_0/A decreases as [O_2] increases. The work in this thesis chapter explains the cause of this anomalous behavior for A_0/A, and the general factors affecting the OH stretch frequency and intensity in alkoxy systems. The difference in absorption cross sections for the OH stretch of HOR• and HOROO• is the main factor causing the observed anomalous behavior for A_0/A. The OH stretch absorption behavior is governed by the relative location of the hydroxy group to the radical center of HOR• or the peroxy group of HOROO•. Quantum chemistry calculations were performed on alcohols (ROH), hydroxyalkyl radicals (HOR•), and hydroxyalkylperoxy radicals (HOROO•), for R = methyl, ethyl, propyl, butyl, and pentyl. OH stretch frequencies and integrated absorption cross sections were calculated at the B3LYP/6-31+G(d,p) level of theory and basis. The results were combined with a kinetics model of the *n*-butoxy system to simulate the apparent A_0/A as a function of [O_2].

Introduction

We have shown in Chapters 7 and 8 that CRDS is capable of measuring the relative kinetics of alkoxy isomerization to reaction with O_2 (k_{isom}/k_{O2}) via the ν_1 (OH stretch band of the primary isomerization products, HOR• (absence of O_2) and HOROO• (presence of O_2). A summary of the results of Chapter 8 are provided here. We measure the relative absorbance A_0/A of the ν_1 band as a function of $[O_2]$, where A is the absorbance for a given O_2, and A_0 is the absorbance for "$[O_2] = 0$" (intercept of regression lines). Considering all of the reactions of alkoxy radicals (RO•, Reactions 9.1–9.5) and hot radicals (RO•*, Reactions 9.6 and 9.7)

$$\text{RO}\bullet \xrightarrow{\text{isom}} \text{HOR}\bullet \tag{9.1}$$

$$\text{RO}\bullet \xrightarrow{\text{isom}}\xrightarrow{+\text{O}_2} \text{HOROO}\bullet \tag{9.2}$$

$$\text{RO}\bullet + \text{O}_2 \longrightarrow \text{R'CHO} + \text{HO}_2 \tag{9.3}$$

$$\text{RO}\bullet \longrightarrow \text{HCHO} + \text{R''}\bullet \tag{9.4}$$

$$\text{RO}\bullet + \text{NO} \longrightarrow \text{RONO} \tag{9.5}$$

$$[\text{RO}\bullet]^* \xrightarrow{\text{prompt isom}} \text{HOR}\bullet \xrightarrow{+\text{O}_2} \text{HOROO}\bullet \tag{9.6}$$

$$[\text{RO}\bullet]^* \xrightarrow{\text{prompt decomp}} \text{HCHO} + \text{R''}\bullet \tag{9.7}$$

we obtain Equations 9.8–9.11: the relationship of A_0/A vs $[O_2]$ and the value of k_{isom}/k_{O2}.

$$\frac{A_0}{A} = \frac{\left(\dfrac{\dfrac{k_{O_2}}{k_{isom}}}{1+\dfrac{k_{NO}[\text{NO}]}{k_{isom}}+\dfrac{k_{decomp}}{k_{isom}}}\right)[\text{O}_2]+1}{\left(\dfrac{\phi_{pi}\dfrac{k_{O_2}}{k_{isom}}}{1+\phi_{pi}\left(\dfrac{k_{NO}[\text{NO}]}{k_{isom}}+\dfrac{k_{decomp}}{k_{isom}}\right)}\right)[\text{O}_2]+1} \tag{9.8}$$

$$\frac{k_{isom}}{k_{O_2}} = \left[\left(\frac{\partial\left(\frac{A_0}{A}\right)}{\partial[\mathrm{O_2}]} \right)_{[\mathrm{O_2}]=0} \right]^{-1} \times X_{kin} \times X_{prompt}, \tag{9.9}$$

where

$$X_{kin} = \frac{1}{1 + \frac{k_{decomp}}{k_{isom}} + \frac{k_{NO}[\mathrm{NO}]}{k_{isom}}}, \tag{9.10}$$

$$X_{prompt} = \frac{(1-\phi_{pi})}{1 + \phi_{pi}\left(\frac{k_{decomp}}{k_{isom}} + \frac{k_{NO}[\mathrm{NO}]}{k_{isom}} \right)}. \tag{9.11}$$

Since ϕ_{pi} (prompt isomerization fraction) was determined to be much less than 1 (4% for *n*-butoxy, 5% for 2-pentoxy), Equation 9.8 shows that A_0/A will increase as $[\mathrm{O_2}]$ increases. Figure 9.1 shows the relative kinetics data for *n*-butoxy, as measured by the ν_1 bands of HOR• and HOROO•. For $[\mathrm{O_2}] > 3 \times 10^{16}$ molec cm^{-3}, we observe the trend predicted by Equation 9.8: an increase in A_0/A with increasing $[\mathrm{O_2}]$. However, we do not observe the trend predicted by Equation 9.8 at low $[\mathrm{O_2}]$. For $0 < [\mathrm{O_2}] < 3 \times 10^{16}$ molec cm^{-3}, we observe a decrease in A_0/A with increasing $[\mathrm{O_2}]$. Furthermore, Equation 9.8 predicts $A_0/A = 1$ for $[\mathrm{O_2}] = 0$; however, in Figure 9.1, we observe $A_0/A = 1.2$ at $[\mathrm{O_2}] = 0$.

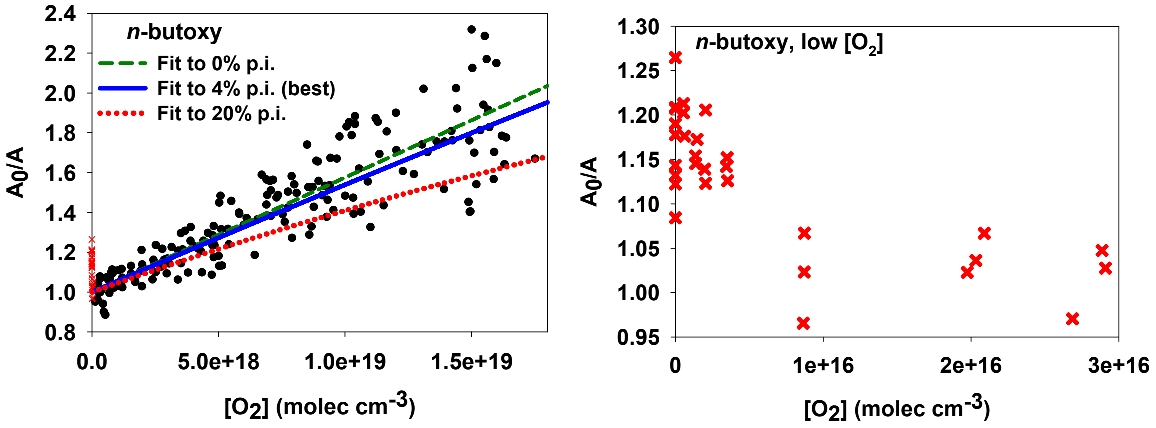

Figure 9.1. A_0/A plotted as a function of $[O_2]$ for *n*-butoxy using the ν_1 CRDS absorbance (Chapter 7). For $[O_2] > 3 \times 10^{16}$ molec cm^{-3} (black markers), we observe the expected decrease in A/A_0 with $[O_2]$. For $0 < [O_2] < 3 \times 10^{16}$ molec cm^{-3}, the *n*-butoxy data show an apparent increase in A/A_0 with $[O_2]$ (points marked by red Xs on the left panel, expanded in the right panel). Because of this effect, only absorbance data with $[O_2] > 1 \times 10^{17}$ molec cm^{-3} were used in the fits to determine k_{isom}/k_{O2} (Chapter 8). Adapted with permission from Sprague et al.[31] Copyright 2012 American Chemical Society.

One explanation for this behavior is that different isomerization products are detected in each $[O_2]$ regime. When $[O_2]$ far exceeds [HOR•], then addition of O_2 to the isomerization product (Reaction 9.2) is immediate. Thus, any spectroscopic measurement of the "isomerization product" is actually a measurement of HOROO•. In contrast, at very low O_2, the amount of HOR• that reacts with O_2 is small (or none, for $[O_2] = 0$). In this case, the primary "isomerization product" being detected is HOR•. We have already observed in Chapter 7 that the ν_1 bands of HOR• and HOROO• have different intensities and shapes. This effect may be one of the causes of nonlinearity in the plot of A_0/A vs $[O_2]$ at low $[O_2]$, where the identity of the isomerization product changes from HOR• to HOROO•. Additionally, these two species are only the primary products of alkoxy isomerization. The relative kinetics measurements presented in Figure 9.1 were made 110 μs after the initial formation of alkoxy radicals. As discussed in Chapter 8, secondary products form in appreciable quantities on this timescale. For example, at [RO•] = 2×10^{14} molec cm^{-3} and [O_2] = 0, 50% of the isomerization product HOR• can self-react to form HORROH (Chapter 8). If the spectroscopic properties of these secondary products differ significantly from HOR• and HOROO•, then we must account for the presence of these products. Thus, in order to fully interpret the relative kinetics data presented in Chapter 8, a theoretical analysis of the primary and secondary products is necessary (spectroscopy, modeled concentrations, simulated A_0/A vs [O_2]).

If the OH stretch absorption changes between the HOR• and HOROO• formed from alkoxy chemistry, a larger chemical physics question is presented: how does the OH stretch absorption vary as a function of the relative positions of the hydroxy group and peroxy group/radical center? This question arises due to the contrasting behavior observed for δ-HOC_4H_8•/δ-HOC_4H_8OO• (Chapter 7) and $HOCH_2OO$• (HMP) (Chapter 4). We have observed that the OH stretch frequencies of δ-HOC_4H_8•, δ-HOC_4H_8OO• and *n*-butanol are all approximately the same (3675 cm^{-1} for the radicals, 3671 cm^{-1} for *n*-butanol). In contrast, the OH stretch of HMP is red shifted by 70 cm^{-1} compared to methanol (3611 cm^{-1} for HMP, 3681 cm^{-1} for methanol). It is possible that the band position changes because of the relative location of the peroxy and hydroxy groups (far apart for the butoxy case, on the same carbon for HMP). This idea makes sense based on the argument that the dipole derivative should change greatly if the peroxy group is interacting with the hydroxy group, either through the overall electronic structure or by hydrogen bonding. However, no calculations on these hydroxyalkylperoxy systems have been performed to support this idea. Although other groups have computed harmonic vibrational frequencies,[19-21, 108, 111, 136-138] these calculations were used only to obtain a zero-point vibrational energy: individual frequencies and intensities were not reported.

In this thesis chapter, we describe a combined quantum chemical and kinetics modeling study to determine the spectroscopic properties of the chemical species formed during alkoxy reactions. Our focus is on the harmonic frequency and integrated intensity of the OH stretch vibrational mode. Although the motivation for this study comes from our work on *n*-butoxy and 2-pentoxy, we also seek to answer the larger chemical physics questions of whether similar behavior persists with different sized alkoxy radicals, and what factors determine the OH stretch absorption behavior. To determine the effect of carbon chain length on the spectroscopic properties, we examine the species ROH, HOR•, and HOROO• for R = methyl, ethyl, *n*-propyl, *n*-butyl, *n*-pentyl, and isopentyl. To determine the effect of the relative positions of the hydroxy group and the peroxy group/radical center, we examine ROH, HOR•, and HOROO• for various straight chain isomers of R = pentyl. We then constructed a kinetics model for the reactions of *n*-butoxy, performed further quantum chemical calculations on any -OH containing species within the model, and simulated the strength of the OH stretch spectroscopic band based on the kinetics model and harmonic frequencies. These results were used to construct a plot of the apparent A_0/A vs $[O_2]$ for comparison to the relative kinetics data presented in Chapter 8.

Methods

Kinetics Model

As observed by the modeling in Chapters 7 and 8, secondary products of alkoxy isomerization contribute to the observed OH stretch intensity. It is necessary to determine what products form and to what extent they form over the entire range of [O_2] used in the relative kinetics experiment, so that all of the observed intensity is accounted for. In order to determine what chemical species are being detected, we constructed a kinetics model for the reactions of *n*-butoxy radical. All kinetics modeling was performed in Kintecus 3.95.[191] Table 9.1 summarizes the reactions and rate constants used in the kinetics model. Most of the rate constants are taken from the JPL Data Evaluation, IUPAC Kinetics database, and the NIST Kinetics database.[27, 117, 118] The rate constant for *n*-butoxy isomerization is based on our measured $k_{\mathrm{isom}}/k_{\mathrm{O2}}$ from Chapter 8, since it is these data that we seek to explain. The impact of choosing a different $k_{\mathrm{isom}}/k_{\mathrm{O2}}$ is explored in the *Discussion* section.

Note that this model is much larger than necessary to correctly model alkoxy chemistry over 110 μs. This design was intentional; the model is capable of modeling chemistry over milliseconds, as was illustrated in Chapters 7 and 8.

Table 9.1. Kinetics Model for *n*-butoxy. Rate constants were taken from JPL,[27] IUPAC,[118] or estimated from similar reactions in NIST,[117] unless otherwise specified

$A^{a,b}$	***Ea*/*R* (K)**	**reaction**	**source**
1) Alkoxy Primary Reactions			
2.37E+05	0	C4H9O==>HOC4H8	Chapter 8
5.80E+02	0	C4H9O==>C3H7+HCHO	Atkinson[142]
1.40E−14	0	C4H9O+O2==>C3H7CHO+HO2	Atkinson[142]
2) Association with O_2			
7.50E−12	0	HOC4H8+O2==>HOC4H8OO	IUPAC

8.00E−12	0	C3H7+O2==>C3H7OO	IUPAC
3) Additional peroxy formation by HO_2+HCHO			
9.70E−15	−625	HO2+HCHO==>HOCH2OO	JPL
4) Peroxy destruction by NO			
9.00E−12	0	HOC4H8OO+NO==>HOC4H8O+NO2	IUPAC, NIST
4.00E−13	0	HOC4H8OO+NO==>HOC4H8ONO2	NIST
9.00E−12	0	C3H7OO+NO==>C3H7O+NO2	IUPAC, NIST
4.00E−13	0	C3H7OO+NO==>C3H7ONO2	NIST
2.80E−12	−300	HOCH2OO+NO==>HOCH2O+NO2	JPL
4.00E−13	0	HOCH2OO+NO==>HOCH2ONO2	JPL
5) Alkyl radical dimerization or association			
5.00E−11	0	HOC4H8+HOC4H8==>HOC8H16OH	NIST
1.69E−11	0	C3H7+C3H7==>C6H14	NIST
1.55E−10	0	C4H9+C4H9==>C4H10+C4H8	NIST
1.70E−11	0	HOC3H6+HOC3H6==>HOC6H12OH	similar to NIST
1.00E−12	0	HOC3H6CH(OH)+HOC3H6CH(OH)==>HOC3H6CHO+ HOC4H8OH	similar to NIST
1.70E−11	0	HOC4H8+C3H7==>C7H15OH	similar to NIST
1.70E−11	0	HOC4H8+C4H9==>C8H17OH	similar to NIST
1.70E−11	0	HOC4H8+HOC3H6==>HOC7H14OH	similar to NIST
5.00E−12	0	HOC4H8+HOC3H6CH(OH)==>C4H9OH+HOC3H6CHO	similar to NIST
1.70E−11	0	C3H7+C4H9==>C7H16	similar to NIST
1.70E−11	0	C3H7+HOC3H6==>C6H13OH	similar to NIST
5.00E−12	0	C3H7+HOC3H6CH(OH)==>C3H8+HOC3H6CHO	similar to NIST
1.70E−11	0	C4H9+HOC3H6==>C7H15OH	similar to NIST
5.00E−12	0	C4H9+HOC3H6CH(OH)==>C4H10+HOC3H6CHO	similar to NIST
5.00E−12	0	HOC3H6+HOC3H6CH(OH)==>C3H7OH+HOC3H6CHO	similar to NIST
6) Peroxy Self Reactions			
5.00E−13	0	HOC4H8OO+HOC4H8OO==>HOC4H8O+HOC4H8O+O2	NIST
7.80E−14	−1000	C3H7OO+C3H7OO==>C3H7O+C3H7O+O2	IUPAC
5.50E−12	0	HOCH2OO+HOCH2OO==>HOCH2O+HOCH2O+O2	IUPAC
5.70E−14	−750	HOCH2OO+HOCH2OO==>HCOOH+HOCH2OH+O2	IUPAC
3.50E−13	−430	HO2+HO2==>H2O2+O2	JPL
1.70E−33	−1000	HO2+HO2+M==>H2O2+O2+M	JPL
7) Peroxy Cross Reactions			
5.00E−13	0	HOC4H8OO+C3H7OO==>HOC4H8O+C3H7O+O2	NIST
5.00E−13	0	HOC4H8OO+HOCH2OO==>HOC4H8O+HOCH2O+O2	NIST
8.00E−12	0	HOC4H8OO+HO2==>HOC4H8OOH+O2	JPL
5.00E−13	0	C3H7OO+HOCH2OO==>C3H7O+HOCH2O+O2	NIST
8.00E−12	0	C3H7OO+HO2==>C3H7OOH+O2	JPL
1.20E−11	0	HOCH2OO+HO2==>HOCH2OOH+O2	IUPAC
8) $RONO_2$ Eliminations			
1.60E−12	0	HOC4H8ONO2+OH==>HONO2+HOC4H8O	IUPAC
5.80E−13	0	C3H7ONO2+OH==>HONO2+C3H7O	IUPAC
3.00E−13	0	HOCH2ONO2+OH==>HONO2+HOCH2O	NIST
9) HORO and smaller RO reactions			
1.58E+11	3270	HOC4H8O==>HOC3H6CH(OH)	NIST
2.00E+13	9560	HOC4H8O==>HCHO+HOC3H6	NIST
1.40E−14	0	HOC4H8O+O2==>HO2+HOC3H6CHO	NIST
2.60E−11	0	HOC3H6CH(OH)+O2==>HOC3H6CHO+HO2	NIST
5.00E+13	7850	C3H7O==>HCHO+C2H5	NIST
2.60E−14	253	C3H7O+O2==>HO2+C2H5CHO	IUPAC
7.80E−12	0	C2H5+O2==>C2H5OO	IUPAC
3.80E−15	0	C2H5+O2==>C2H4+HO2	IUPAC

7.50E−12	0	HOC3H6+O2==>HOC3H6OO	IUPAC
10) Reactions with NO: Alkoxy and small peroxies			
3.32E−11	0	C4H9O+NO==>C4H9ONO	NIST
3.30E−11	0	HOC4H8O+NO==>HOC4H8ONO	NIST
4.00E−11	0	HOCH2O+NO==>HOCH2ONO	NIST
3.80E−11	0	C3H7O+NO==>C3H7ONO	IUPAC
9.00E−12	0	C2H5OO+NO==>C2H5O+NO2	NIST
1.60E−15	16.78	C2H5OO+NO==>C2H5ONO2	NIST
9.00E−12	0	HOC3H6OO+NO==>HOC3H6O+NO2	NIST
4.00E−13	0	HOC3H6OO+NO==>HOC3H6ONO2	NIST
11) Alkyl Reactions with NO			
6.64E−14	0	HOC4H8+NO==>HOC4H8NO	NIST
6.64E−14	0	C3H7+NO==>C3H7NO	NIST
6.51E−12	0	HOC3H6CH(OH)+NO==>HOC3H6CHO+HNO	NIST
6.64E−14	0	HOC3H6+NO==>HOC3H6NO	NIST
2.30E−13	0	C2H5+NO==>C2H5NO	NIST
12) Alkyl Reactions with HO_2			
4.00E−11	0	C4H9+HO2==>C4H9O+OH	NIST
4.00E−11	0	HOC4H8+HO2==>HOC4H8O+OH	NIST
4.00E−11	0	C3H7+HO2==>C3H7O+OH	NIST
4.00E−11	0	HOC3H6+HO2==>HOC3H6O+OH	NIST
2.60E−11	0	HOC3H6CH(OH)+HO2==>HOC3H6CHO+H2O2	NIST
13) Alkyl Nitrite reaction with OH			
2.00E−12	0	C4H9ONO+OH==>C4H9+HONO2	NIST
2.00E−12	0	C4H9ONO+OH==>C4H9O+HONO	NIST
14) Butyl and butyl peroxy reactions with NO, OH, and other peroxies			
6.64E−14	0	C4H9+NO==>C4H9NO	NIST
7.50E−12	0	C4H9+O2==>C4H9OO	IUPAC
9.00E−12	0	C4H9OO+NO==>C4H9O+NO2	IUPAC
4.00E−13	0	C4H9OO+NO==>C4H9ONO2	NIST
1.60E−12	0	C4H9ONO2+OH==>C4H9O+HONO2	IUPAC
4.00E−13	0	C4H9OO+C4H9OO==>C4H9O+C4H9O+O2	NIST
5.00E−13	0	C4H9OO+HOC4H8OO==>C4H9O+HOC4H8O+O2	NIST
5.00E−13	0	C4H9OO+C3H7OO==>C4H9O+C3H7O+O2	NIST
5.00E−13	0	C4H9OO+HOCH2OO==>C4H9O+HOCH2O+O2	NIST
15) Peroxy reactions with alkyl			
4.00E−11	0	C4H9OO+C4H9==>C4H9O+C4H9O	NIST
4.00E−11	0	C4H9OO+HOC4H8==>HOC4H8O+C4H9O	NIST
4.00E−11	0	C4H9OO+C3H7==>C3H7O+C4H9O	NIST
4.00E−11	0	C4H9OO+HOC3H6==>C4H9O+HOC3H6O	NIST
4.00E−11	0	HOC4H8OO+C4H9==>HOC4H8O+C4H9O	NIST
4.00E−11	0	HOC4H8OO+HOC4H8==>HOC4H8O+HOC4H8O	NIST
4.00E−11	0	HOC4H8OO+C3H7==>HOC4H8O+C3H7O	NIST
4.00E−11	0	HOC4H8OO+HOC3H6==>HOC4H8O+HOC3H6O	NIST
4.00E−11	0	C3H7OO+C4H9==>C3H7O+C4H9O	NIST
4.00E−11	0	C3H7OO+HOC4H8==>C3H7O+HOC4H8O	NIST
4.00E−11	0	C3H7OO+C3H7==>C3H7O+C3H7O	NIST
4.00E−11	0	C3H7OO+HOC3H6==>C3H7O+HOC3H6O	NIST
4.00E−11	0	HOCH2OO+C4H9==>HOCH2O+C4H9O	NIST
4.00E−11	0	HOCH2OO+HOC4H8==>HOCH2O+HOC4H8O	NIST
4.00E−11	0	HOCH2OO+C3H7==>HOCH2O+C3H7O	NIST
4.00E−11	0	HOCH2OO+HOC3H6==>HOCH2O+HOC3H6O	NIST
1.00E−11	0	C4H9OO+HOC3H6CH(OH)==>C4H9OOH+HOC3H6CHO	NIST

1.00E−11	0	HOC4H8OO+HOC3H6CH(OH)==>HOC4H8OOH+ HOC3H6CHO	NIST
1.00E−11	0	C3H7OO+HOC3H6CH(OH)==>C3H7OOH+HOC3H6CHO	NIST
1.00E−11	0	HOCH2OO+HOC3H6CH(OH)==>HOCH2OOH+ HOC3H6CHO	NIST
16) Peroxy reactions with alkoxy			
2.00E−12	0	HOC4H8OO+C4H9O==>HOC4H8OOH+C3H7CHO	NIST
2.00E−12	0	HOC4H8OO+HOC4H8O==>HOC4H8OOH+HOC3H6CHO	NIST
2.00E−12	0	HOC4H8OO+C3H7O==>HOC4H8OOH+C2H5CHO	NIST
2.00E−12	0	HOC4H8OO+HOCH2O==>HOC4H8OOH+HCOOH	NIST
2.00E−12	0	C4H9OO+C4H9O==>C4H9OOH+C3H7CHO	NIST
2.00E−12	0	C4H9OO+HOC4H8O==>C4H9OOH+HOC3H6CHO	NIST
2.00E−12	0	C4H9OO+C3H7O==>C4H9OOH+C2H5CHO	NIST
2.00E−12	0	C4H9OO+HOCH2O==>C4H9OOH+HCOOH	NIST
2.00E−12	0	C3H7OO+C4H9O==>C3H7OOH+C3H7CHO	NIST
2.00E−12	0	C3H7OO+HOC4H8O==>C3H7OOH+HOC3H6CHO	NIST
2.00E−12	0	C3H7OO+C3H7O==>C3H7OOH+C2H5CHO	NIST
2.00E−12	0	C3H7OO+HOCH2O==>C3H7OOH+HCOOH	NIST
2.00E−12	0	HOCH2OO+C4H9O==>HOCH2OOH+C3H7CHO	NIST
2.00E−12	0	HOCH2OO+HOC4H8O==>HOCH2OOH+HOC3H6CHO	NIST
2.00E−12	0	HOCH2OO+C3H7O==>HOCH2OOH+C2H5CHO	NIST
2.00E−12	0	HOCH2OO+HOCH2O==>HOCH2OOH+HCOOH	NIST
17) Peroxy reactions with OH			
1.00E−10	0	C4H9OO+OH==>C4H9OH+O2	NIST
1.00E−10	0	HOC4H8OO+OH==>HOC4H8OH+O2	NIST
1.00E−10	0	C3H7OO+OH==>C3H7OH+O2	NIST
1.00E−10	0	HOCH2OO+OH==>HOCH2OH+O2	NIST
1.00E−10	0	C2H5OO+OH==>C2H5OH+O2	NIST
18) HO$_x$ and NO$_x$ chemistry (from the Global Kinetics Model used for Part 3 of this thesis)			
1.61E−12	0	OH+NO2==>HOONO	JPL
7.22E−01	0	HOONO==>OH+NO2	JPL
1.07E−12	0	HO2+NO2==>HO2NO2	JPL
6.67E−02	0	HO2NO2==>HO2+NO2	JPL
6.73E−15	0	NO+NO2==>N2O3	JPL
3.22E+05	0	N2O3==>NO+NO2	JPL
2.59E−14	0	NO2+NO2==>N2O4	JPL
9.13E+04	0	N2O4==>NO2+NO2	JPL
1.17E−12	0	NO2+NO3==>N2O5	JPL
4.02E−02	0	N2O5==>NO2+NO3	JPL
5.88E−12	0	OH+OH==>H2O2	JPL
6.90E−12	0	OH+NO==>HONO	JPL
9.99E−12	0	OH+NO2==>HONO2	JPL
1.80E−12	0	OH+OH==>H2O+O	JPL
4.80E−11	−250	OH+HO2==>H2O+O2	JPL
1.80E−12	0	OH+H2O2==>H2O+HO2	JPL
3.50E−12	−250	HO2+NO==>OH+NO2	JPL

a) Units of *A* are cm^3 molec^{-1} s^{-1} for bimolecular reactions, and s^{-1} for unimolecular reactions

b) Termolecular reactions have already been converted to the effective bimolecular rate constant: the listed rate constants are valid at 670 torr, 298 K only

The initial conditions used for the kinetics simulations are summarized in Table 9.2. These conditions (gas concentrations, temperature, total pressure) were chosen to match the experimental conditions used in the experiments described in Chapter 8. Briefly, *n*-butoxy was formed in the reaction cell by photolysis of *n*-butyl nitrite (C_4H_9ONO) using 351 nm light. Approximately 1% of C_4H_9ONO was photolyzed. For typical $[C_4H_9ONO]_0$ of 2×10^{16} molec cm^{-3}, the resulting *n*-butoxy concentration was 2×10^{14} molec cm^{-3}. We ran simulations for $[O_2] = 0$ and for the range 1×10^{13} molec cm^{-3} to 2×10^{19} molec cm^{-3} (four $[O_2]$ values per order of magnitude). Simulations were run for 110 μs, with an integration step size of 5 ns. The concentration of all OH containing species at 110 μs was recorded for each $[O_2]$.

Table 9.2. Kinetics Model Parameters

Parameter	Value
$[C_4H_9ONO]_0$	2×10^{16} molec cm^{-3}
$[C_4H_9O]_0$	2×10^{14} molec cm^{-3}
$[NO]_0$	2×10^{14} molec cm^{-3}
$[O_2]_0$	$(0\text{–}2.17) \times 10^{19}$ molec cm^{-3} [a]
$[N_2]_0$	$(0\text{–}2.17) \times 10^{19}$ molec cm^{-3} [a]
Total Pressure	670 torr
Temperature	298 K
Simulation Time	110 μs
Integration Step Size	5 ns

a) The sum of $[O_2]$ and $[N_2]$ was kept constant at 2.17×10^{19} molec cm^{-3}

Quantum Chemistry Calculations

Our strategy for choosing which chemical species to run calculations on consists of three parts. We would like to examine whether carbon chain length affects the OH stretch absorption properties amongst hydroxyalkyl and hydroxyalkylperoxy radicals. We therefore chose to run calculations on the primary products (HOR• and HOROO•) and parent alcohols (ROH), for a variety of alkane chain lengths (up to five carbons). To obtain chemical species similar to the ones observed in alkoxy isomerization, we placed the hydroxy group and radical center/peroxy group on opposite ends of the carbon chain. Secondly, we wish to investigate how the relative positions of the hydroxy group and the peroxy group/radical center affect the OH stretch position and intensity. To accomplish this, we ran calculations on all of the straight carbon chain isomers of pentanol, hydroxypentyl, and hydroxypentylperoxy. Finally, we would like to determine the OH stretch absorption properties of all relevant species within our kinetics model. We therefore chose to run calculations on all species within the *n*-butoxy kinetics model that contain an OH stretch.

Table 9.3 contains the chemical species that we examined for this study. All quantum chemistry calculations were performed in Gaussian 03W,[79] on a single processor, dual core workstation. Geometry optimizations and harmonic frequency calculations were performed at the B3LYP/6-31+G(d,p) level of theory and basis. Molecules with three or fewer carbons were also analyzed at CCSD/6-31+G(d,p) to ensure that the relative intensities were independent of the level of theory. We did not choose to scale any of the frequencies or intensities, as we are only interested in the relative OH stretch band positions and absorption cross sections. The "`Density=Current`" command was used in all calculations to ensure that the B3LYP or CCSD wavefunction was used to perform orbital population and electric dipole analysis (details in Appendix C). Additionally, multiple conformers of the *n*-butoxy system were analyzed to determine whether or not different conformers would have different relative intensities.

Table 9.3. Chemical Species Calculated for This Study

Part 1: Carbon Chain Size Study (ROH, HOR•, HOROO•) B3LYP/6-31+G(d,p)		
Alcohol	Hydroxyalkyl	Hydroxyalkylperoxy
CH_3OH	$HOCH_2\bullet$	$HOCH_2OO\bullet$
CH_3CH_2OH	$HOCH_2CH_2\bullet$	$HOCH_2CH_2OO\bullet$
$CH_3CH_2CH_2OH$	$HOCH_2CH_2CH_2\bullet$	$HOCH_2CH_2CH_2OO\bullet$
$CH_3CH_2CH_2CH_2OH$	$HOCH_2CH_2CH_2CH_2\bullet$	$HOCH_2CH_2CH_2CH_2\bullet$
$CH_3CH_2CH_2CH_2CH_2OH$	$HOCH_2CH_2CH_2CH_2CH_2\bullet$	$HOCH_2CH_2CH_2CH_2CH_2\bullet$
$CH_3CH_2CH_2CH(OH)CH_3$	$CH_3CH(OH)CH_2CH_2CH_2\bullet$	$CH_3CH(OH)CH_2CH_2CH_2OO\bullet$
Part 2: Check that B3LYP and CCSD give similar results CCSD/6-31+G(d,p)		
Alcohol	Hydroxyalkyl	Hydroxyalkylperoxy
CH_3OH	$HOCH_2\bullet$	$HOCH_2OO\bullet$
CH_3CH_2OH	$HOCH_2CH_2\bullet$	$HOCH_2CH_2OO\bullet$
$CH_3CH_2CH_2OH$	$HOCH_2CH_2CH_2\bullet$	$HOCH_2CH_2CH_2OO\bullet$
Part 3: Change relative positions of OO and OH groups on pentoxy system B3LYP/6-31+G(d,p)		
Alcohol	Hydroxyalkyl	Hydroxyalkylperoxy
$CH_3CH_2CH_2CH_2CH_2OH$	$\bullet CH_2CH_2CH_2CH_2CH_2OH$	$\bullet OOCH_2CH_2CH_2CH_2CH_2OH$
	$CH_3CH(\bullet)CH_2CH_2CH_2OH$	$CH_3CH(OO\bullet)CH_2CH_2CH_2OH$
	$CH_3CH_2CH(\bullet)CH_2CH_2OH$	$CH_3CH_2CH(OO\bullet)CH_2CH_2OH$
	$CH_3CH_2CH_2CH(\bullet)CH_2OH$	$CH_3CH_2CH_2CH(OO\bullet)CH_2OH$
	$CH_3CH_2CH_2CH_2CH(\bullet)OH$	$CH_3CH_2CH_2CH_2CH(OO\bullet)OH$
$CH_3CH_2CH_2CH(OH)CH_3$	$\bullet CH_2CH_2CH_2CH(OH)CH_3$	$\bullet OOCH_2CH_2CH_2CH(OH)CH_3$
	$CH_3CH(\bullet)CH_2CH(OH)CH_3$	$CH_3CH(OO\bullet)CH_2CH(OH)CH_3$
	$CH_3CH_2CH(\bullet)CH(OH)CH_3$	$CH_3CH_2CH(\bullet)CH(OH)CH_3$
	$CH_3CH_2CH_2C(\bullet)(OH)CH_3$	$CH_3CH_2CH_2C(OO\bullet)(OH)CH_3$
	$CH_3CH_2CH_2CH(OH)CH_2\bullet$	$CH_3CH_2CH_2CH(OH)CH_2OO\bullet$
$CH_3CH_2CH(OH)CH_2CH_3$	$\bullet CH_2CH_2CH(OH)CH_2CH_3$	$\bullet OOCH_2CH_2CH(OH)CH_2CH_3$
	$CH_3CH(\bullet)CH(OH)CH_2CH_3$	$CH_3CH(OO\bullet)CH(OH)CH_2CH_3$
	$CH_3CH_2C(\bullet)(OH)CH_2CH_3$	$CH_3CH_2C(OO\bullet)(OH)CH_2CH_3$
Part 4: OH containing molecules in the *n*-butoxy system B3LYP/6-31+G(d,p)		
Alcohols, Diols	Hydroxyalkyl, Hydroxyalkylperoxy	Hydroxyalkoxy, Hydroxyalkylperoxide
C_3H_7OH	$HOC_4H_8\bullet$	$HOC_4H_8O\bullet$
$C_7H_{15}OH$	$HOC_4H_8OO\bullet$	HOC_4H_8OOH
HOC_4H_8OH		C_3H_7OOH
$HOC_8H_{16}OH$		

The frequencies and integrated intensities for each OH stretch mode were recorded. For the *n*-butoxy system, these integrated intensities were entered into the kinetics model to determine the overall OH stretch absorption. These overall absorptions were scaled to the cross section of δ-HOC_4H_8OO• to obtain an apparent A_0/A for use in our plots of A_0/A vs [O_2].

Results

We present the results of this study in three parts. First, we present the kinetics simulations of the *n*-butoxy system at [O_2] = 0 and [O_2] = 2.17×10^{19} molec cm^{-3}. The results of the kinetics simulations show us that only 50%–81% of the –OH containing products at 110 μs exist as the primary isomerization products HOR• or HOROO•, depending on [O_2]. The results show that self-reaction of HOR• at low [O_2] is very important. At high [O_2], secondary products make up 25% of the total –OH containing species, attributable to the stable end-products HOR'CHO, HOROOH, and HOROH. Second, we present the quantum chemical calculations on the ν_1 (OH stretch) harmonic frequencies and intensities. These results give us insight into how carbon chain length and relative position of the hydroxy group and the peroxy group/radical center affect the OH stretch absorption properties. We observe that addition of the peroxy group to a hydroxyalkyl radical will increase the OH stretch intensity by 15%–20%, with deviant behavior observed when both the hydroxy and peroxy groups are located on the same or adjacent carbons. Most of the secondary products have cross sections similar to the hydroxyalkyl radicals: only the hydroxyalkylperoxy radicals have a higher cross section. Finally, we combine the quantum chemical cross sections with the *n*-butoxy kinetics simulations to build up the plot of A_0/A vs [O_2], analogous to the plot presented in Chapter 8. Our simulations are able to simultaneously reproduce the low [O_2] anomaly and provide a good fit to the relative kinetics data, indicating that the primary cause of the low [O_2] anomaly in Figure 9.1 is the change in products being detected as [O_2] is increased.

Kinetics Model for n-butoxy

The concentrations of OH containing species from our kinetics model are shown in Figure 9.2, for [O_2] = 0 (left) and [O_2] = 2.17×10^{19} molec cm^{-3} (right), for the first 110 μs after formation of the *n*-butoxy radicals. Although full kinetics data exist for all of the [O_2] that we examined, we examine these two concentrations in full detail to determine the major products and important secondary chemistry for low and high [O_2].

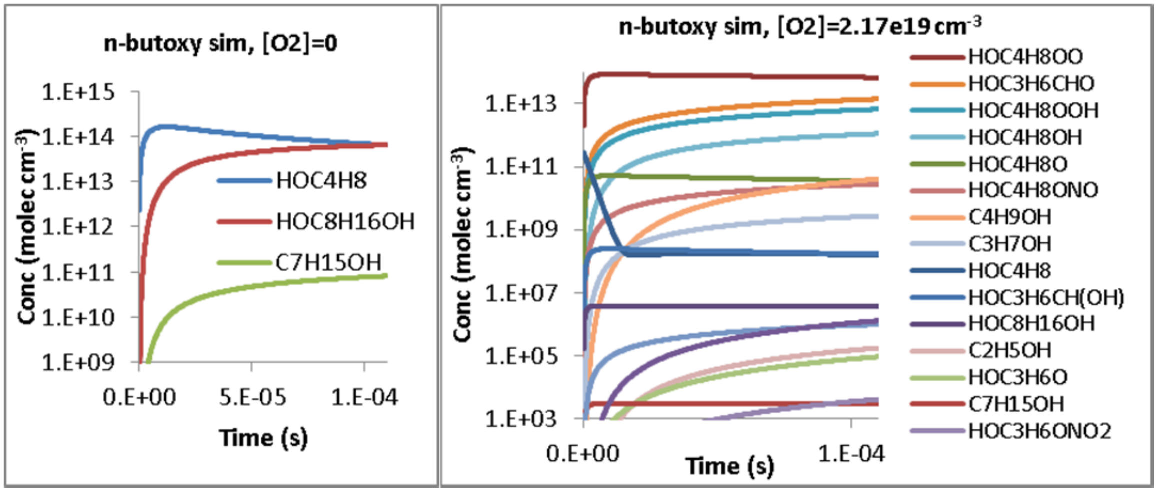

Figure 9.2. Concentration (log scale) vs time for the OH containing chemical species in the *n*-butoxy kinetics model, for [O_2] = 0 (left) and [O_2] = 2.17×10^{19} molec cm^{-3} (right).

The kinetics simulations allow us to answer the question "What isomerization product is being detected at 110 μs?" At [O_2] = 0, only three products are being detected. 50% of the isomerization product exists as HOC_4H_8•, the direct product of isomerization (Reaction 9.1). 50% of the isomerization product exists as 1,8-octanediol ($HOC_8H_{16}OH$), formed from the self-reaction of HOC_4H_8• (Reaction 9.12).

$$\mathrm{HOR\bullet + HOR\bullet \longrightarrow HORROH} \quad (9.12)$$

n-heptanol ($C_7H_{15}OH$), a minor product accounting for less than 0.05% of the total isomerization product, forms from reaction of the decomposition product C_3H_7• with the direct isomerization product HOC_4H_8• (Reaction 9.13).

$$\bullet\mathrm{C_3H_7} + \bullet\mathrm{C_4H_8OH} \longrightarrow \mathrm{C_7H_{15}OH} \quad (9.13)$$

In contrast to the low [O_2] kinetics data, we observe the formation of many different secondary products for [O_2] = 2.17×10^{19} molec cm^{-3}. Most of these products are present in small concentrations: the four products in highest concentration account for 99.9% of the OH stretch containing species. As expected, very little of the isomerization product exists as HOC_4H_8•, and the major product observed is HOC_4H_8OO• (Reaction 9.2), accounting for 75% of the observed products with OH groups.

The remaining three species are stable end-products on the isomerization pathway. 16% of the products exist as hydroxybutanal (HOC_3H_6CHO), formed through multiple series of reactions. This product is one of the "classic" molecules detected in end-product studies,[155, 161] yet it forms in appreciable quantities even within 110 μs. 7% of the isomerization product exists as a hydroperoxide, HOC_4H_8OOH. The hydroperoxide forms from the reaction of HOC_4H_8OO• with the HO_2 formed from reaction of the alkoxy radical with O_2 (Reactions 9.3 and 9.14).

$$\mathrm{HO_2\bullet + HOROO\bullet \longrightarrow HOROOH + O_2} \quad (9.14)$$

1% of the products exist as 1,4-*n*-butyldiol (HOC_4H_8OH), formed from the reaction of HOROO• with OH. The OH is formed when one of the decomposition products (C_3H_7•) reacts with the HO_2 from Reaction 9.9 (Reactions 9.4, 9.3, 9.15, 9.16).

$$\mathrm{R'\bullet + HO_2 \longrightarrow R'O\bullet + OH} \quad (9.15)$$

$$\mathrm{HOROO\bullet + OH \longrightarrow HOROH + O_2} \tag{9.16}$$

The remaining products in Figure 9.3b account for less than 0.1% of the OH containing product concentration. Their effect on the OH stretch spectrum of the alkoxy products is therefore expected to be negligible. Of particular note is the fact that the three major products for $[O_2] = 0$ ($HOC_4H_8\bullet$, $HOC_8H_{16}OH$, $C_7H_{15}OH$) are now in negligible concentrations for $[O_2] = 2.17 \times 10^{19}$ molec cm^{-3}. This makes it absolutely clear that the isomerization products being detected change greatly as a function of $[O_2]$.

Knowing that the detected isomerization products are different for low and high $[O_2]$, we now address the question of how the nature of the detected products changes as a function of $[O_2]$. Figure 9.3 shows the percentage of each –OH containing product at 110 μs as a function of $[O_2]$, comparing the amount of primary product (defined as HOR• and HOROO•) to secondary product (defined as HORROH, HOR'CHO, HOROH, and HOROOH) (Figure 9.3a), the amount of HOR• to HOROO• (Figure 9.3b), and the amounts of each secondary product (Figures 9.3c and 9.3d).

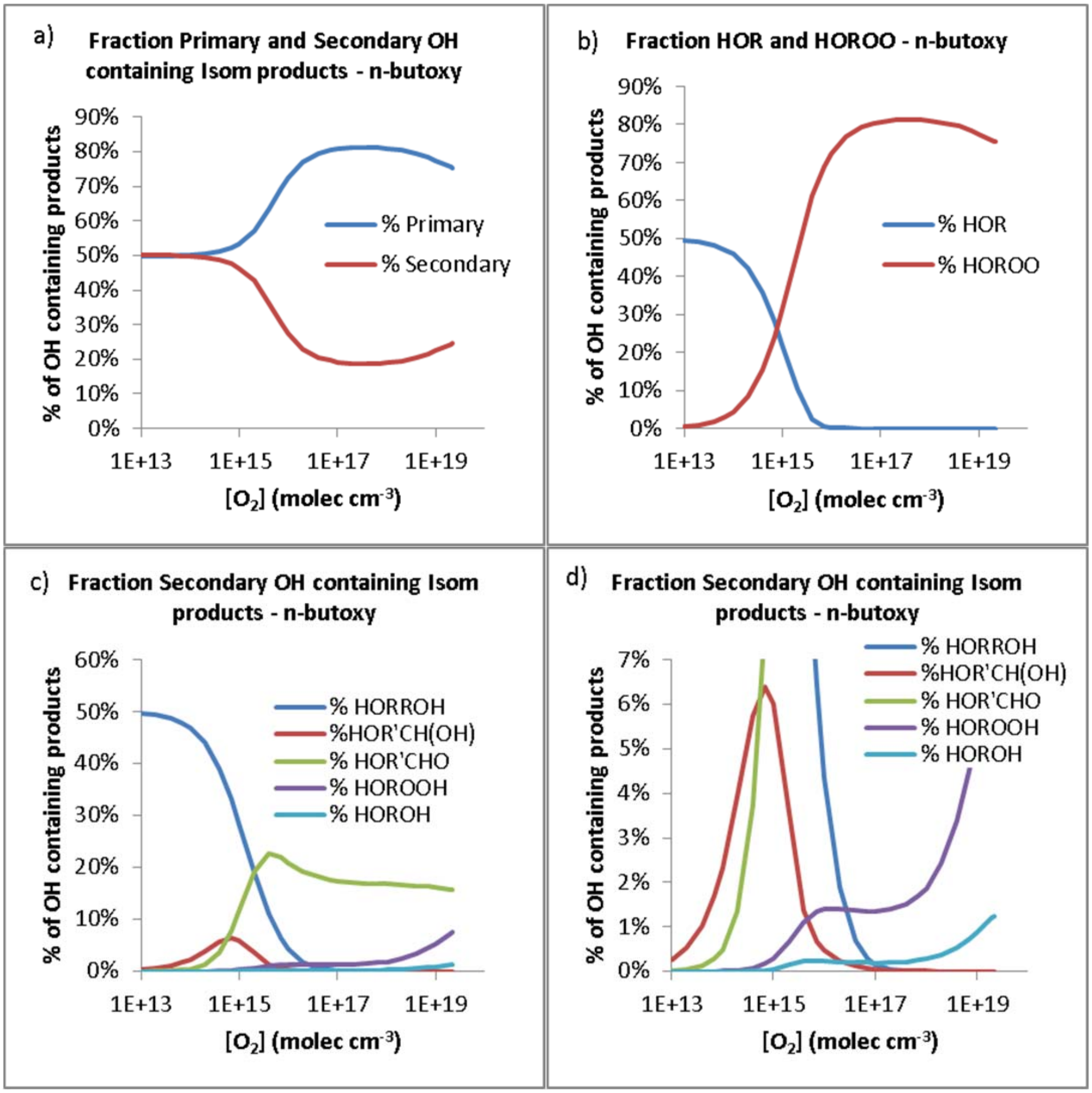

Figure 9.3. Description of the –OH containing products of the *n*-butoxy chemical system at 110 μs, as a function of O_2. The plots show the percentage of –OH containing species that each individual chemical contributes. Part (a) shows the percentage of –OH containing molecules that exist as primary isomerization products (HOR•, HOROO•) and secondary isomerization products (HORROH, HOROH, HOR'CHO, HOR'CH•(OH) and HOROOH), where R = C_4H_8. Part (b) shows the distribution of primary products. Parts (c) and (d) show the distribution of secondary products.

On the basis of Figure 9.3, we can describe what isomerization products are being detected for each [O_2]. For [O_2] < 10^{14} molec cm^{-3}, 50% of the product exists as HOR•, and 50% exists as $HOC_8H_{16}OH$. In the range 10^{14} molec cm^{-3} < [O_2] < 10^{17} molec cm^{-3}, the distribution of isomerization products changes rapidly. The percentage of secondary products decreases rapidly (to 20% at $[O_2] = 10^{17}$ molec cm^{-3}). Meanwhile, the primary products change from HOR• to HOROO•, with nearly all primary product existing as HOROO• at $[O_2] = 10^{16}$ molec cm^{-3}. For $[O_2] > 10^{16}$ molec cm^{-3}, most of the products remain as HOROO•, with a slight decrease in relative abundance with $[O_2]$ (81% at $[O_2] = 10^{17}$ molec cm^{-3}, 75% at $[O_2] = 2.17 \times 10^{19}$ molec cm^{-3}). The secondary products are present in significant concentrations, and their relative abundances change with $[O_2]$. The dominant secondary product for $[O_2] > 10^{16}$ molec cm^{-3} is the stable end-product HOR'CHO. For $[O_2] > 10^{18}$ molec cm^{-3}, [HOROOH] becomes appreciable, rising from 2%–7% over the range (1–21) × 10^{18} molec cm^{-3}.

Considering all of the kinetics data in Figure 9.3, we observe that secondary chemistry effects affect the 110 μs CRDS experiment at all $[O_2]$, with the largest fraction of secondary products observed for $[O_2] < 10^{16}$ molec cm^{-3}. We also note that the identity of the primary product changes rapidly from HOR• to HOROO• as $[O_2]$ is increased over the range 10^{14}–10^{16} molec cm^{-3}. Careful attention is needed when interpreting alkoxy isomerization data for $[O_2] < 10^{16}$ molec cm^{-3}. In contrast, we note that the distribution of products remains relatively constant over the range 10^{17} molec cm^{-3} < $[O_2]$ < 10^{19} molec cm^{-3}. For these values of $[O_2]$, minimal changes in the OH spectrum due to changing products will be observed. This justifies the procedures in Chapter 8 of only performing linear regression on relative kinetics data with 10^{17} molec cm^{-3} < $[O_2]$ < 10^{19} molec cm^{-3}.

Quantum Chemical Calculations

The results of the quantum chemical calculations can be divided into five parts. First, we examine how the carbon chain length affects the OH stretch absorption properties for species with up to five carbons. In order to obtain compounds most relevant to alkoxy isomerization studies, we only look at isomers with the hydroxy group and radical center/peroxy group as far away as possible. Second, we show that the relative frequencies and intensities of the OH stretch do not change when the level of theory is increased from B3LYP to CCSD. This result allows us to use the faster B3LYP calculations to accurately analyze the OH stretch properties. Third, we show that the OH stretch properties are not significantly changed amongst different conformers of the *n*-butoxy isomerization products. Fourth, we examine the dependence of the OH stretch properties on the relative positions of the hydroxy and radical center/peroxy groups for a straight chain pentyl backbone. The results show that the main factor governing the relative OH stretch properties is the relative positions of the hydroxy group and radical center/peroxy groups, while the second most important factor is the absolute position of the groups on the carbon chain. Fifth, we calculate the OH stretch frequencies and intensities of all –OH containing species in the *n*-butoxy chemical system. These data will then be combined with the kinetics model to interpret Garland's CRDS measurements.

Effect of carbon chain size on OH stretch properties

One of the goals of this study was to answer the general chemical physics question of how the OH stretch frequency and intensity differs between an alcohol

(ROH), a hydroxyalkyl radical (HOR•), and a hydroxyalkyl peroxy radical (HOROO•), and how the OH stretch is affected by alkyl chain length. Table 9.4 summarizes the harmonic frequencies (ω_e) and intensities (I) of these chemical species, for R = methyl, ethyl, *n*-propyl, *n*-butyl, *n*-pentyl, and isopentyl. For these species, the hydroxy group and radical center/peroxy group were placed on opposite ends of the carbon chain, in order to obtain chemical species that best resemble products of alkoxy isomerization. In particular, the *n*-butyl and isopentyl chemical species were reported in Chapters 7 and 8, and these calculations provide insight into what factors affect those experiments.

Table 9.4. Harmonic frequencies and intensities for straight chain alcohols, alkoxy radicals, and hydroxyalkylperoxy radicals, at B3LYP/6-31+G(d,p).

R	ROH		HOR•		HOROO•		
	ω_e^{a}	I^a	ω_e^{a}	I^a	ω_e^{a}	I^a	$I_{HOROO\bullet}/I_{HOR\bullet}$
Methyl	3839	28	3839	59	3799	53	0.9
Ethyl	3836	26	3836	26	3844	46	1.8
n-propyl	3836	26	3839	30	3836	35	1.2
n-butyl	3841	29	3841	30	3842	35	1.2
n-pentyl	3835	25	3834	25	3836	30	1.2
isopentyl	3828	20	3828	21	3829	25	1.2

a) Harmonic frequencies are in cm^{-1}, intensities are in km mol^{-1}

Examination of the frequencies and intensities in Table 9.4 reveals different behavior for R = methyl, R = ethyl, and all larger R groups. Considering R = methyl, we notice that the OH stretch position is the same for CH_3OH and $HOCH_2$•, while the OH stretch is red shifted for $HOCH_2OO$• by 40 cm^{-1}. This is in qualitative agreement with the OH stretch spectrum of HMP presented in Chapter 4, where we observed a 60 cm^{-1} red shift compared to methanol. We also notice that the integrated intensities of the OH stretch for $HOCH_2$• and $HOCH_2OO$• are nearly twice as large as for CH_3OH. In contrast to this behavior, for R = ethyl, we notice that the OH stretch frequencies of C_2H_5OH and

HOC_2H_4• are roughly equal, while HOC_2H_4OO• is blue shifted by 8 cm^{-1}. The integrated intensity of the OH stretch is roughly constant for C_2H_5OH and HOC_2H_4•, while the intensity nearly doubles for HOC_2H_4OO•. It is likely that the relative proximity of the hydroxyl group to the radical center or peroxy group is causing the large changes in intensity and frequencies (as will be shown later for the different isomers for R = pentyl).

The remaining species in Table 9.4 (R = *n*-propyl, *n*-butyl, *n*-pentyl, isopentyl) exhibit similar behavior when comparing ROH, HOR•, and HOROO•. For these R groups, the OH stretch frequency does not change between the three chemical species. In all cases, addition of the peroxy group increases the integrated intensity by a factor of 15–20%. For all of these R groups except *n*-C_3H_7, ROH and HOR• have the same integrated intensity. The similarity in OH stretch behavior amongst the different alkyl groups suggests that when the hydroxyl group and radical center or peroxy group are far enough apart, the OH stretch is only affected by the large change in dipole that occurs upon addition of a peroxy group.

Spectroscopic Properties as a Function of Level of Theory and Basis

Before embarking on any further analysis of the calculations, we must ensure that the relative trends in OH stretch frequency and intensity are not affected by the level of theory that we are using. B3LYP is a relatively cheap method, and can be used to study larger alkoxy systems without the need for a supercomputer. More sophisticated methods, such as CCSD, will presumably be more accurate with respect to spectroscopic properties. The problem is that CCSD frequency calculations are relatively expensive due to the lack of analytical gradients in Gaussian 03W,[79] and can only be used to study smaller alkoxy systems. As an illustration of this point, the harmonic frequency calculation for $HOC_3H_6OO\bullet$ took 2100 times as much cpu time at CCSD/6-31+G(d,p) than at B3LYP/6-31+G(d,p). Because the cpu scaling of CCSD is of order N^6 (where N = number of basis functions), CCSD calculations on butyl and pentyl systems are both outside of the reach of our 32-bit, single processor workstation. However, if the OH stretch properties are in agreement between the two methods, then we can feel comfortable using the B3LYP results for larger systems (butyl or larger) where CCSD calculations would be unfeasible.

Table 9.5 contains the OH stretch harmonic frequencies and intensities at B3LYP/6-31+G(d,p) and CCSD/6-31+G(d,p) for ROH, HOR•, and HOROO•, for R = methyl, ethyl, and *n*-propyl. For these species, the hydroxy group and radical center/peroxy group were placed on opposite ends of the carbon chain in order to obtain chemical species that best resemble products of alkoxy isomerization. The B3LYP results are listed normally while the CCSD results are in parentheses. We expect the absolute frequencies and intensities to differ between the two methods; however, if B3LYP is an acceptable level of theory, the relative intensities amongst ROH, HOR•, and HOROO• should be the same for B3LYP and CCSD. We immediately notice that the trends in harmonic frequencies between ROH, HOR•, and HOROO• is the same between the two methods. Additionally, the ratio of intensities is roughly the same between the two methods. The generally good agreement between the two methods suggests that we can trust our B3LYP results for all of the systems being studied.

Table 9.5. Harmonic frequencies and intensities for straight chain alcohols, alkoxy radicals, and hydroxyalkylperoxy radicals, at B3LYP/6-31+G(d,p) (top), and CCSD/6-31+G(d,p) (bottom, in parentheses).

R	ROH		HOR•		HOROO•		
	ω_e^a	I^a	ω_e^a	I^a	ω_e^a	I^a	$I_{HOROO•}/I_{HOR•}$
Methyl	3839 (3912)	28 (26)	3839 (3913)	59 (53)	3799 (3884)	53 (50)	0.9 (1.0)
Ethyl	3836 (3905)	26 (24)	3835 (3904)	26 (24)	3844 (3913)	46 (42)	1.8 (1.7)
n-propyl	3836 (3903)	26 (24)	3839 (3905)	30 (27)	3836 (3902)	35 (32)	1.2 (1.2)

a) Harmonic frequencies are in cm^{-1}, intensities are in km mol^{-1}

Similarly, we can also investigate how sensitive the relative frequencies and relative intensities are to the choice of basis set. Table 9.6 compares the B3LYP frequencies and intensities for two basis sets: 6-31+G(d,p) (plain numbers) and aug-cc-pVTZ (in parentheses). We observe very little change in relative frequencies and intensities upon changing the basis set, indicating that our choice of 6-31+G(d,p) will be adequate for our study.

Table 9.6. Harmonic Frequencies and Intensities for straight chain alcohols, alkoxy radicals, and hydroxyalkylperoxy radicals, at B3LYP/6-31+G(d,p) (top), and B3LYP/aug-cc-pVTZ (bottom, in parentheses).

R	ROH		HOR•		HOROO•		
	ω_e^a	I^a	ω_e^a	I^a	ω_e^a	I^a	$I_{HOROO•}/I_{HOR•}$
Methyl	3839 (3829)	28 (31)	3839 (3824)	59 (62)	3799 (3785)	53 (53)	0.9 (0.9)
Ethyl	3836 (3825)	26 (29)	3835 (3827)	26 (31)	3844 (3833)	46 (49)	1.8 (1.6)
n-propyl	3836 (3827)	26 (30)	3839 (3829)	30 (34)	3836 (3826)	35 (39)	1.2 (1.1)

a) Harmonic frequencies are in cm^{-1}, intensities are in km mol^{-1}

Comparison of n-butoxy Conformer OH Stretch Properties

It is also possible that the relative OH stretch frequencies and intensities of ROH, HOR•, and HOROO• change based on the conformation of the molecule. It is important to account for this effect, since in our cavity ringdown experiments, alkoxy radicals are formed from photolysis of an alkyl nitrite (Reaction 9.17, $\Delta H = 40$ kcal mol^{-1}),[186] giving 40 kcal mol^{-1} of excess energy to be distributed between the RO• and NO fragments.

$$\text{RONO} \xrightarrow{h\nu = 351\text{ nm}} \text{RO}\bullet + \text{NO} \tag{9.17}$$

Excess energy leading to population of multiple conformers is not limited to our study; any experiment utilizing photolysis of alkyl nitrites will have the same issue, notably if the photolysis energy is much higher than 40 kcal mol^{-1}.[29, 30] It is therefore plausible that multiple conformers of HOR• and HOROO• will be present in the experiment. We must check whether or not the ratio of intensities for our primary products, $I_{\text{HOROO}\bullet}/I_{\text{HOR}\bullet}$, remains constant amongst different conformers. If $I_{\text{HOROO}\bullet}/I_{\text{HOR}\bullet}$ remains constant or only changes slightly, then the observed OH stretch intensity will be a simple function of which chemical species are present. If $I_{\text{HOROO}\bullet}/I_{\text{HOR}\bullet}$ changes greatly, then the observed OH stretch intensity will be convoluted by the conformational distribution, which would have to be accounted for in our analysis.

Table 9.7 contains the OH stretch harmonic frequencies and intensities for four different conformers of δ-HOC_4H_8• and δ-HOC_4H_8OO radical, calculated at B3LYP/6-31+G(d,p). To differentiate between conformers, the energy relative to Conformer 1 (the lowest energy conformer of δ-HOC_4H_8• examined) is also reported. We notice that amongst the first three conformers, the OH stretch harmonic frequencies remains nearly constant, only changing by ±2 cm^{-1}. The intensities also remain nearly constant, and so does $I_{\mathrm{HOROO}\bullet}/I_{\mathrm{HOR}\bullet}$. All three of these conformers have some bending in the carbon backbone. In contrast, the fourth conformer has its harmonic frequencies red shifted by about 10 cm^{-1} compared to the other conformers. Additionally, the OH stretch intensity of δ-HOC_4H_8• is only 25 km mol^{-1}, much lower than the other conformers (30 km mol^{-1}). This reduction in OH stretch intensity leads to a larger intensity ratio $I_{\mathrm{HOROO}\bullet}/I_{\mathrm{HOR}\bullet}$ (1.3 for Conformer 4, 1.2 for the other three). A more exhaustive search of conformers would be necessary to obtain a single value of $I_{\mathrm{HOROO}\bullet}/I_{\mathrm{HOR}\bullet}$ that would best represent the OH stretch intensity change between δ-HOC_4H_8OO• and δ-HOC_4H_8•. However, most of our calculated conformers yield the same absolute intensities and $I_{\mathrm{HOROO}\bullet}/I_{\mathrm{HOR}\bullet}$. We will therefore use the intensities for Conformer 1 in our kinetics analysis, with the caveat that a larger conformer search must be performed in order to obtain more accurate cross sections.

Table 9.7. Relative energies (no zero-point energy correction), harmonic frequencies, and intensities for conformers of δ-HOC_4H_8• and δ-HOC_4H_8OO•, at B3LYP/6-31+G(d,p).

		HOC_4H_8•		HOC_4H_8OO•		
Conformer	energy[a]	ω_e[b]	I[b]	ω_e[b]	I[b]	$I_{\mathrm{HOROO}\bullet}/I_{\mathrm{HOR}\bullet}$
1	0	3841	30	3842	35	1.2
2	93	3843	31	3839	35	1.2
3	94	3843	31	3841	35	1.2
4	169	3833	25	3836	32	1.3

a) The listed energies are the energy of δ-HOC_4H_8• relative to Conformer 1, in cm^{-1}.
b) Harmonic frequencies are in cm^{-1}, intensities are in km mol^{-1}.

Effect of functional group positions on the OH stretch properties

We now turn our attention to how the relative positions of the hydroxy group and the radical center/peroxy group affect the trends in OH stretch frequency and intensity. In Table 9.4, we observed that the relative OH stretch properties for ROH, HOR•, and HOROO• were different for R = methyl, R = ethyl, and R = propyl or larger. It is plausible that the different behavior is due to the strength of interaction between the hydroxy group and the radical center/peroxy group, whether this interaction is a hydrogen bond or simply an electrostatic interaction. One way to test this idea is to compute the OH stretch frequencies and intensities for a large number of isomers with the same carbon backbone (in this case, *n*-pentyl), where each isomer differs in the placement of the hydroxy group and the radical center/peroxy group. If proximity of the two functional groups is the main reason for the different behavior between R = methyl, R = ethyl, and R = propyl or larger, then we should see a similar result in our pentyl isomer calculations. When the hydroxy and radical center/peroxy group are on the same carbon, we should see OH stretch behavior similar to that of R = methyl. Likewise, when the hydroxy group and radical center/peroxy groups are on adjacent carbons, we should see OH stretch behavior similar to R = ethyl. When the two groups are even further apart, we should see OH stretch behavior similar to R = propyl or larger.

Table 9.8 contains the harmonic frequencies and intensities for the straight carbon chain isomers of pentanol, hydroxypentyl radical, and hydroxypentylperoxy. The positions of the hydroxy group and radical center/peroxy group for each isomer are listed in the first two columns. The data in the table have been sorted according to how far away the hydroxy group and radical center/peroxy groups are. In addition, the frequencies and intensities of the smaller hydroxyalkylperoxy radicals from Table 9.4 have also been included in order to compare radicals of different sizes.

Note: It is useful to adopt a numbering scheme to make discussing these molecules easier. Let {x, y} represent the straight chain isomer of HOC_5H_{10}• or

$HOC_5H_{10}OO\bullet$ with the OH group on carbon x, and the radical center or OO group on carbon y.

Table 9.8. Harmonic Frequencies and Intensities for straight chain isomers of pentanol, hydroxypentyl radicals, and hydroxypentylperoxy radicals, at B3LYP/6-31+G(d,p).

Positions		$C_5H_{11}OH$		$HOC_5H_{10}\bullet$		$HOC_5H_{10}OO\bullet$		
OH	OO	ω_e^a	I^a	ω_e^a	I^a	ω_e^a	I^a	$I_{HOROO\bullet}/I_{HOR\bullet}$
OH on same carbon as radical/peroxy								
methyl		3839	28	3839	59	3799	53	0.9
1	1	3835	25	3839	57	3780	53	0.9
2	2	3828	20	3824	36	3749	53	1.5
3	3	3838	20	3826	39	3652	86	2.2
OH one carbon away from radical/peroxy								
ethyl		3836	26	3836	26	3844	46	1.8
1	2	3835	25	3835	24	3848	43	1.8
2	3	3828	20	3820	15	3835	29	1.9
2	1	3828	20	3819	23	3755	69	3.0
3	2	3838	20	3812	10	3839	27	2.8
OH two carbons away from radical/peroxy								
n-propyl		3836	26	3839	30	3836	35	1.2
1	3	3835	25	3838	29	3839	34	1.2
2	4	3828	20	3827	22	3826	25	1.2
3	1	3838	20	3839	22	3836	26	1.2
OH three carbons away from radical/peroxy								
n-butyl		3841	29	3841	30	3842	35	1.2
1	4	3835	25	3835	26	3837	30	1.2
2	5	3828	20	3828	21	3829	25	1.2
OH four carbons away from radical/peroxy								
1	5	3835	25	3834	25	3835	30	1.2

a) Harmonic frequencies are in cm^{-1}, intensities are in km mol^{-1}

To first order, the data in Table 9.8 show different OH stretch behavior depending on the relative location of the hydroxy group and the radical center/peroxy group. We group these results into three categories: OH and OO are 1) on the same carbon, 2) on adjacent carbons, or 3) further than one carbon apart.

OH and OO on same carbon: For all three of these molecules, we notice that the OH stretch of HOROO• is red shifted compared to HOR•. The magnitude of the red shift increases as the functional groups are moved toward the center of the chain (40 cm^{-1} for

{1, 1}, 75 cm^{-1} for {2, 2}, and 175 cm^{-1} for {3, 3}). This red shift is due to a hydrogen bond between the OH and OO groups, analogous to the red shifts observed in the OH stretch spectra of HOONO (Chapter 3)[12, 15, 42, 43, 70, 74-76, 88] and HMP (Chapter 4). Furthermore, we can also make a comparison between R = methyl and the {1, 1} isomer, since both molecules have the two functional groups on the end carbon. The harmonic frequencies follow the same trend (ROH = HOR•, HOROO• red shifted by 40 cm^{-1}). Additionally, the OH stretch intensities follow the same ratio (intensity of HOR• and HOROO• is twice as large as ROH, and $I_{\mathrm{HOROO\bullet}}/I_{\mathrm{HOR\bullet}} = 0.9$). Evidently, when both functional groups are on the end carbon, the OH stretch behavior is exactly the same as the R = methyl case. However, when a middle carbon holds both functional groups, vastly different trends for the OH stretch are observed. For the {2, 2} isomer, the OH stretch intensity of HOR• is twice as large as ROH, while $I_{\mathrm{HOROO\bullet}}$ is three times as large as I_{ROH}. Meanwhile, the harmonic frequencies of ROH and HOR• are the same, while HOROO• is red shifted by 75 cm^{-1}. In contrast, for the {3, 3} isomer, the OH stretch intensity of HOR• is less than that of ROH, while HOROO• has an intensity twice as large as ROH. The harmonic frequencies also follow a different pattern, with ROH > HOR• > HOROO•. Additionally, the ratio $I_{\mathrm{HOROO\bullet}}/I_{\mathrm{HOR\bullet}}$ increases as the functional groups move towards the middle of the carbon chain (0.9 for {1, 1}, 1.5 for {2, 2}, and 2.2 for {3, 3}).When both functional groups are on the same carbon, the absolute position of the functional groups along the carbon chain determines the properties of the OH stretch.

OH and OO on adjacent carbons: We notice two separate trends based on the absolute ordering of the functional groups: one when the hydroxy group is closer to the end of the carbon chain than the radical center/peroxy group ({1, 2} and {2, 3}), and a second when the radical center/peroxy group is closer to the end of the carbon chain than the hydroxy group ({2, 1} and {3, 2}). First consider the {1, 2} and {2, 3} isomers. The OH stretch harmonic frequency of HOROO• is blue shifted by 15 cm^{-1} compared to HOR•. Additionally, the ratio $I_{\mathrm{HOROO}\bullet}/I_{\mathrm{HOR}\bullet}$ is approximately the same for both of these molecules (1.8 for {1, 2}, 1.9 for {2, 3}). We also notice that comparing HOR• to HOROO•, both {1, 2} and {2, 3} have similar changes to the R = ethyl case from Table 9.4. The ratio $I_{\mathrm{HOROO}\bullet}/I_{\mathrm{HOR}\bullet}$ is similar in magnitude for all three species, and all three species have HOROO• blue shifted compared to HOR•, suggesting similar properties for the OH stretch. However, the trends between ROH and HOR• differ between the two isomers. The {1, 2} isomer shows no change in harmonic frequency, and only a 5% decrease in intensity. In contrast, the {2, 3} isomer has the OH stretch of HOR• red shifted by 7 cm^{-1} compared to ROH, while the intensity decreased by 20%.

Very different behavior is observed when the radical center/peroxy group is closer to the end of the carbon chain than the hydroxy group, as is the case for the {2, 1} and {3, 2} isomers. Both isomers have roughly the same $I_{\mathrm{HOROO}\bullet}/I_{\mathrm{HOR}\bullet}$ (3.0 for {2, 1}, 2.8 for {3, 2}), and both isomers have HOR• blue shifted compared to ROH (8 cm^{-1} for {2, 1}, 65 cm^{-1} for {3, 2}). The similarities between the {2, 1} and {3, 2} isomers end here, however. The {2, 1} isomer has the HOROO• harmonic frequency blue shifted by 65 cm^{-1} compared to HOR•, while the {3,2} isomer has the HOROO• harmonic frequency red shifted by 25 cm^{-1} compared to HOR•. Additionally, the OH stretch intensities do not follow the same patterns. The {2, 1} isomer has $I_{\mathrm{ROH}} < I_{\mathrm{HOR}\bullet} << I_{\mathrm{HOROO}\bullet}$, while the {3, 2} isomer has $I_{\mathrm{HOR}\bullet} << I_{\mathrm{HOROO}\bullet} < I_{\mathrm{ROH}}$. Although the intensity trend for HOR• and HOROO•

is the same between the {2, 1} and {3, 2} isomers, most of the properties follow different trends.

OH and OO on nonadjacent carbons: All of the chemical species in this section ({1, 3}, {2, 4}, {3, 1} {1, 4}, {2, 5}, {1, 5}) follow the same OH stretch trends. The harmonic frequencies of ROH, HOR•, and HOROO• are all the same to ±3 cm^{-1}. The absorption intensities all follow the same pattern, with $I_{\text{ROH}} < I_{\text{HOR}\bullet} < I_{\text{HOROO}\bullet}$. The ratio $I_{\text{HOROO}\bullet} / I_{\text{HOR}\bullet}$ is the same for all of these chemical species (1.2). Finally, these isomers have essentially the same properties as the *n*-propyl and *n*-butyl species calculated in Table 9.4. Our conclusion is that the OH stretch properties behave in the same manner when the hydroxy group and radical center/peroxy group are further than one carbon apart.

Looking at the entire data set, we note that there are two main factors affecting the OH stretch behavior. First, the distance between the hydroxy group and the radical center/peroxy group is the dominant factor determining the OH stretch behavior. When the two functional groups are sufficiently far enough apart (two or more carbons), the same harmonic frequency and intensity relationships are observed between ROH, HOR•, and HOROO•, regardless of chain length or absolute positions of the functional groups. When the functional groups are closer (same carbon or adjacent carbons), a second factor comes into play: how close the functional groups are to the end of the carbon chain. We notice very different behavior in the adjacent carbon cases when the peroxy group is closer to the end of the chain than when the hydroxy group is closer to the end of the chain. Similarly, for the same carbon case, the absolute position of the functional groups changes the OH stretch behavior between ROH, HOR•, and HOROO•.

Calculation of OH Stretch Properties for the Kinetics Model

We now examine the –OH containing chemical species in our *n*-butoxy kinetics model. Two types of OH groups are present: alcohols (–OH) and peroxides (–OOH), and both groups must be accounted for in our calculations. As seen in the *Kinetics Model* section, the dominant products contributing to the OH stretch band will be HOC_4H_8• and HOC_4H_8OO•, both of which have a similar harmonic frequency (3841 cm^{-1} for HOC_4H_8•, 3842 cm^{-1} for HOC_4H_8OO•). If any other chemical species in the reaction mechanism also have OH stretches with similar frequencies, then they will contribute intensity to the observed OH stretch band. On the other hand, if the OH stretch frequencies are far from HOC_4H_8• and HOC_4H_8OO•, then the species will not contribute any intensity to the observed peak. Table 9.9 contains the OH stretch harmonic frequencies and intensities for the –OH containing species in the *n*-butoxy kinetics model.

Table 9.9. Harmonic Frequencies and Intensities for the hydroxyl containing species in the *n*-butoxy kinetics model, at B3LYP/6-31+G(d,p).

Molecule	$\omega_{e,1}$ [a]	I_1 [a]	$\omega_{e,2}$ [a]	I_2 [a]	Total I at OH str. peak[b]	I per OH group
Major Products, $[O_2] = 0$						
HOC_4H_8•	3841	30	--	--	30	30
$HOC_8H_{16}OH$	3835	51	3835	0	51	26
$C_7H_{15}OH$	3835	25	--	--	25	25
Major Products, $[O_2] > 10^{17}$ molec cm^{-3}						
HOC_4H_8OO•	3842	35	--	--	35	35
HOC_3H_6CHO	3837	32	--	--	32	32
HOC_4H_8OOH	3836	29	3772	48	29	29
HOC_4H_8OH	3834	54	3834	0	54	27
HOC_4H_8O•	3836	28	--	--	28	28
C_4H_9OH	3835	25	--	--	25	25
HOC_3H_6CH•OH	3843	64	3832	22	86	43
Minor Products (total intensity contribution < 0.1%), $[O_2] > 10^{17}$ molec cm^{-3}						
C_3H_7OH	3836	26	--	--	26	26
C_3H_7OOH	--	--	3773	47	0	0.0
$C_8H_{17}OH$	3835	25	--	--	25	25
HOC_3H_6O	3833	29	--	--	29	29
$HOCH_2OH$	3837	33	3807	34	33	33
$C_6H_{13}OH$	3834	25	--	--	25	25
$HOC_7H_{14}OH$	3835	48	3835	3	51	26
HOC_4H_8ONO	3837	31	--	--	31	31
C_2H_5OH	3836	26	--	--	26	26
$HOC_3H_6ONO_2$	3836	37	--	--	37	37
HOC_3H_6NO	3836	34	--	--	34	34

a) Harmonic frequencies are in cm^{-1}, intensities are in km mol^{-1}

b) The total intensity column is the sum of all OH stretch intensities that fall under the HOC_4H_8• peak.

Most of the OH stretches have frequencies within 10 cm^{-1} of HOC_4H_8• and HOC_4H_8OO•, and will therefore contribute intensity to the observed OH stretch peak. These OH stretches are listed in the $\omega_{e,1}$ and I_1 columns. On the other hand, the symmetric OH stretches in the diols, and the peroxide OH stretches (OO-H) do not contribute to the observed OH stretch peak, and are listed in the $\omega_{e,2}$ and I_2 columns. The diol symmetric stretches have near zero intensity, while the peroxide OH stretches are red shifted from the HOC_4H_8• peak by 60 cm^{-1}. As a result, none of these motions can contribute to the observed OH stretch peak. Note, however, that the hydroxy OH stretches of the peroxide molecules do contribute intensity; only the peroxide OH stretch is red shifted.

Simulation of A_0/A vs $[O_2]$

Now that the chemical kinetics and properties of the OH stretch absorption have been calculated, we can simulate the plot of A_0/A vs $[O_2]$ to show that our analysis can fully explain the low $[O_2]$ anomaly in Chapter 8. We do this in the following steps. First, we tabulate the concentrations of all –OH containing species in the kinetics model at 110 μs, for the values of $[O_2]$ used in the *Chemical Kinetics* section. Second, we multiply each of these concentrations by the absorption intensities calculated in the *Quantum Chemistry* section to obtain an overall absorbance. Third, we convert the overall absorbance at each $[O_2]$ to A_0/A using Equation 9.18:

$$\frac{A_0}{A} = \frac{[\mathrm{HOR}\bullet]_0 \, I_{\mathrm{HOROO}\bullet}}{\sum_i c_i I_i}, \tag{9.18}$$

where $[\mathrm{HOR}\bullet]_0$ is the initial concentration of the hydroxybutyl radical (equal to 2×10^{14} molec cm^{-3}), $I_{\mathrm{HOROO}\bullet}$ is the B3LYP/6-31+G(d,p) integrated intensity of the OH stretch for HOC_4H_8OO• (34.9 km mol^{-1}), c_i are the individual concentrations of each OH containing species, and I_i are the integrated intensities of the OH stretches for each OH containing species. The numerator of Equation 9.18 represents the absorbance if 100% of the alkoxy reactant isomerizes ($A_0/A = 1$), while the denominator represents the observed absorbance. The numerator uses $I_{\mathrm{HOROO}\bullet}$ rather than $I_{\mathrm{HOR}\bullet}$ because 1) at large $[O_2]$, nearly all of the products exists as HOROO•, and 2) we used this region of the relative kinetics plot in Chapter 8 to extract $k_{\text{isom}}/k_{\text{O2}}$. We therefore write the apparent A_0/A in terms of HOROO•.

Figure 9.4a shows the apparent A_0/A vs $[O_2]$ data from the simulations performed in this chapter (green line) and our cavity ringdown spectroscopy data (Chapter 8, blue diamonds and red squares), for $[O_2] = (0–1.7) \times 10^{19}$ molec cm^{-3}. In order to better visualize the low $[O_2]$ anomaly, Figure 9.4b zooms in on the region $[O_2] = (0–3) \times 10^{16}$ molec cm^{-3} (CRDS data in the anomaly region in red squares). We notice excellent quantitative agreement between the simulation and our CRDS data. Assuming 10% uncertainty in A_0/A on each data point, the reduced chi-squared statistic (χ_ν^2) is 0.80 over the entire $[O_2]$ range, and 0.64 for $[O_2] < 4 \times 10^{16}$ molec cm^{-3}. Since the values of χ_ν^2 are reasonably close to 1, we have evidence that our kinetics simulation fits well to our CRDS data, and that the estimated error on A_0/A (10%) is appropriate. **The data in Figure 9.4 are good evidence that the combination of quantum chemistry and kinetics modeling can fully explain the low $[O_2]$ anomaly.**

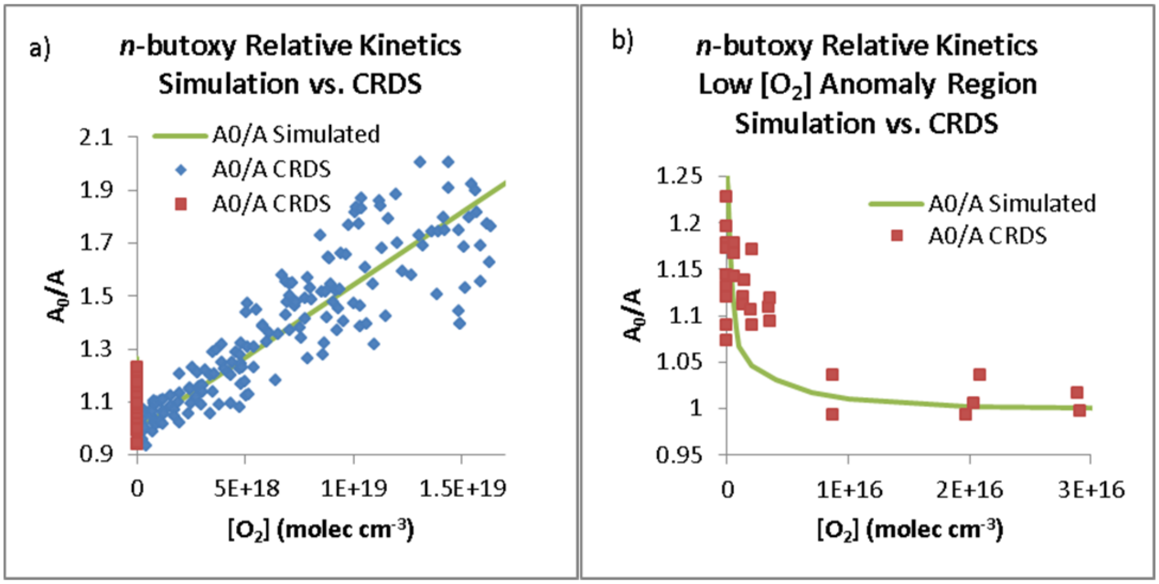

Figure 9.4. Comparison of A_0/A vs [O$_2$] of *n*-butoxy for the relative kinetics simulation (green line) and our cavity ringdown study (blue diamonds and red squares), for [O$_2$] = (0–1.7) × 10^{19} molec cm^{-3} (a), and [O$_2$] = (0–3) × 10^{16} molec cm^{-3} (b). Figure 9.4a shows good quantitative agreement between the simulation and the CRDS data, while Figure 9.4b shows that the kinetics model contains all of the information necessary to explain the low [O$_2$] anomaly observed in our CRDS measurements (Chapter 8). The reduced chi-squared statistic (χ_v^2) is 0.80 over the entire [O$_2$] range, and 0.64 for [O$_2$] < 4 × 10^{16} molec cm^{-3}.

Despite the very good agreement observed in Figure 9.4, it is possible that the CRDS relative kinetics data collection method does not permit a fair comparison between simulation and experiment. About 50% of the relative kinetics data were obtained solely using the OH stretch peak height as a measure of the amount of isomerization product. However, the kinetics modeling presented in this chapter shows that the isomerization products being detected change relative quantities as a function of [O$_2$]. Additionally, the quantum chemical calculations show that the OH stretch frequencies of each isomerization product do not match exactly; the products can differ by as much as ±5 cm^{-1} (see Table 9.9). Although the observed peaks are very wide (FWHM 35–45 cm^{-1}, as shown in Chapter 7), small changes in band position may cause the observed A_0/A to depend on the species being detected. As shown in Figure 9.3, this is most important for $[O_2] > 10^{19}$ molec cm^{-3}, where HOROO• (35 km mol^{-1}) is converted to HOROOH (29 km mol^{-1}).

We can attempt to quantify this change in $k_{\mathrm{isom}}/k_{\mathrm{O2}}$ by refitting our relative kinetics data using only data points that are both unaffected by the low $[O_2]$ anomaly and in the regime where the composition of secondary products is relatively constant (Figure 9.3d). The data points in the region 1×10^{17} molec cm^{-3} < $[O_2]$ < 5×10^{18} molec cm^{-3} satisfy these criteria. The effect of reducing the data set being fit is small. Using the analysis presented in Chapter 8 (correction factor $X_{\mathrm{tot}} = 0.93$) the full data set gives $k_{\mathrm{isom}}/k_{\mathrm{O2}} = (1.69 \pm 0.15) \times 10^{19}$ molec cm^{-3}, while the reduced data set gives $k_{\mathrm{isom}}/k_{\mathrm{O2}} = (1.72 \pm 0.30) \times 10^{19}$ molec cm^{-3}, a change of less than 2%. Since this change is smaller than the statistical scatter in our CRDS data (9%, 2σ), we conclude that our relative rate value $k_{\mathrm{isom}}/k_{\mathrm{O2}}$ is not affected by the changing OH stretch peak positions amongst the isomerization products.

Discussion

With the kinetics and quantum chemistry simulation fully set up, we can address three points of interest. First, it is possible that some of the –OH containing species are not formed from isomerization, but rather through secondary reactions of the O_2 or decomposition pathways. While it may seem plausible that the “extra” OH intensity may partially cause the low $[O_2]$ anomaly, we show that this additional OH stretch intensity is negligible, and thus cannot account for the low $[O_2]$ anomaly. Second, we can compare the results of our full kinetics model to two reduced kinetics model that ignore secondary chemistry. We show that the low $[O_2]$ anomaly persists when we ignore secondary reactions in our model, further evidence that the anomaly is due to the intensity differences between •ROH and •OOROH. Finally, we show that any of the literature $k_{\mathrm{isom}}/k_{\mathrm{O2}}$ will still yield a low $[O_2]$ anomaly, rather than only our value of $k_{\mathrm{isom}}/k_{\mathrm{O2}}$.

Further points of discussion that are worth exploring are the effects of a contaminated sample of *n*-butyl nitrite (in particular, what happens if extra NO is present in the initial nitrite sample), and whether HOC_4H_8OO• can react with the precursor *n*-butyl nitrite. These discussions will be saved for Chapter 10, where they can be put into context based on the kinetics data obtained using the A-X electronic band of HOC_4H_8OO•.

OH groups Formed Through Nonisomerization Pathways

In Chapter 8, we used the OH stretch peak height as a measure of how much alkoxy radical undergoes isomerization. However, not all of the hydroxy groups present 110 μs after alkoxy formation are from the isomerization channel. HO_2 is one of the products from the O_2 channel. This HO_2 can react with NO to form OH and NO_2 (Reaction 9.19). The resulting OH can then react with propylperoxy (Reaction 9.20) or hydroxybutylperoxy (Reaction 9.21) to form species with an OH group. This “extra” OH group will contribute to the absorption peak, but was not formed from isomerization.

$$HO_2 + NO \longrightarrow OH + NO_2 \qquad (9.19)$$

$$OH + C_3H_7OO \longrightarrow C_3H_7OH + O_2 \qquad (9.20)$$

$$OH + HOC_4H_8OO\bullet \longrightarrow HOC_4H_8OH + O_2 \qquad (9.21)$$

The analysis of alkoxy chemistry presented by Sprague et al. states that at high $[O_2]$, less than 2% error in k_{isom}/k_{O2} is introduced.[31] This error is below the statistical uncertainty in k_{isom}/k_{O2} (9%), leading them to conclude that extra OH groups do not impact their analysis of k_{isom}/k_{O2}. One remaining question is whether or not the introduction of "extra" OH groups can account for the low $[O_2]$ anomaly. As $[O_2]$ is increased, the presence of extra OH groups could cause an artificial reduction in A_0/A. At high enough $[O_2]$, if no further extra OH is formed, then the apparent A_0/A will be dominated by the actual k_{isom}/k_{O2}.

To determine whether or not the non-isomerization OH production accounts for the low $[O_2]$ anomaly, we can calculate the fraction of the OH stretch signal that arises from pathways other than isomerization. The only two species in the kinetics model that will contribute nonisomerization intensity are C_3H_7OH and HOC_4H_8OH. We therefore determine the nonisomerization contribution from Equation 9.22:

$$f_{non-isom} = \frac{[\mathrm{C_3H_7OH}]\times I_{\mathrm{C_3H_7OH}} + [\mathrm{HOC_4H_8OH}]\times \frac{1}{2}\times I_{\mathrm{HOC_4H_8OH}}}{\sum \mathrm{c_i} I_\mathrm{i}}\ , \tag{9.22}$$

where $f_{non\text{-}isom}$ is the fraction of OH stretch intensity from nonisomerization channels, I_{C3H7OH} and $I_{HOC4H8OOH}$ are the OH stretch intensities of the two nonisomerization products, c_i are the individual concentrations of the OH containing species, and I_i are the OH stretch intensities for each OH containing species. The factor of ½ accounts for the fact that one of the OH groups on HOC_4H_8OH does form from isomerization. Figure 9.5 shows how $f_{non\text{-}isom}$ varies with $[O_2]$, 100 μs after formation of the *n*-butoxy radical. Figure 9.5a shows the entire range of $[O_2]$, $(0–2) \times 10^{19}$ molec cm^{-3}, while Figure 9.5b zooms in on the $[O_2]$ anomaly region, $(0–4) \times 10^{16}$ molec cm^{-3}. The plots show that

$f_{\text{non-isom}}$ increases nearly monotonically with $[O_2]$, but is less than 1% even at $[O_2] = 2.17 \times 10^{19}$ molec cm^{-3}. In the $[O_2]$ anomaly region, $f_{\text{non-isom}}$ is less than 0.2%, making a negligible contribution to the observed peak. We therefore conclude that nonisomerization –OH containing products are not the cause of the low $[O_2]$ anomaly.

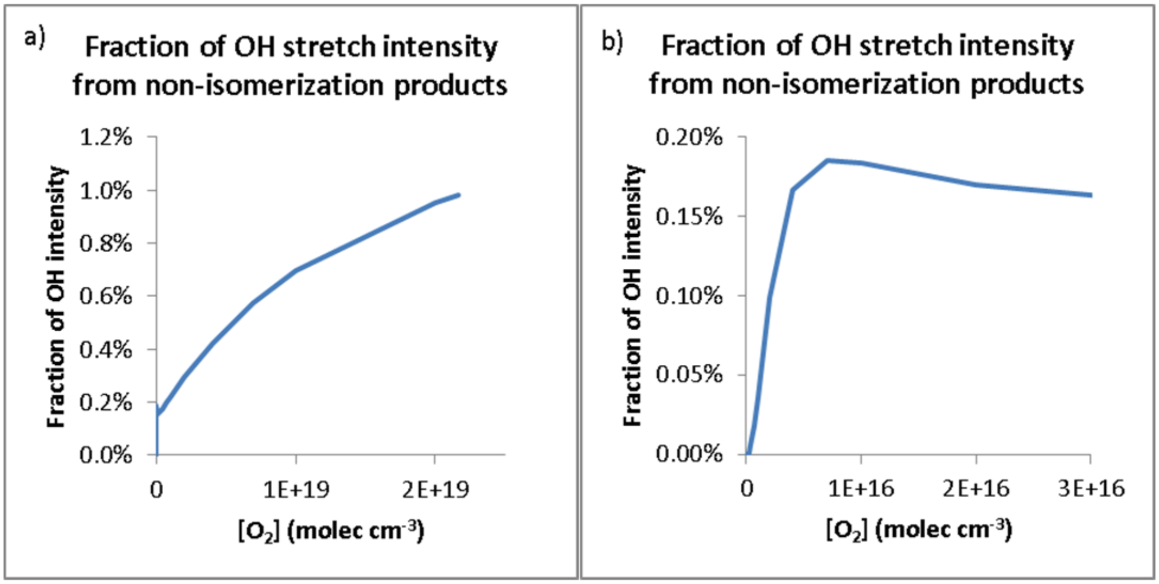

Figure 9.5. Fraction of OH stretch intensity that comes from products formed through non-isomerization reaction pathways, for $[O_2] = (0–2.17) \times 10^{19}$ molec cm^{-3} (a), and $[O_2] = (0–4) \times 10^{16}$ molec cm^{-3} (b). Part a shows that the nonisomerization intensity fraction increases nearly monotonically with $[O_2]$. Part b shows that the nonisomerization product contribution to the OH stretch intensity is too small to explain the low $[O_2]$ anomaly.

Reduced Kinetics Model Simulations of A_0/A vs $[O_2]$

Based on the results in the *Quantum Chemistry* section, we postulated that the large change in OH stretch intensity between HOR• and HOROO• was causing the low $[O_2]$ anomaly. The kinetics model also shows that secondary chemistry effects are also important, with the main contributions being from the self-reaction of HOR• to form HORROH at $[O_2] = 0$ and formation of three stable end-products for $[O_2] > 10^{17}$ molec cm^{-3}. It is worthwhile to determine whether the primary alkoxy chemistry alone can fully explain the low [O_2] anomaly, despite not correctly capturing the nature of the secondary products being detected. To test this, we wrote two reduced kinetics models containing only the primary reactions for reaction of *n*-butoxy. These models are listed in Tables 9.10 and 9.11. The reactions included in both models are decomposition, isomerization, reaction with O_2, reaction with NO, and association of O_2 with the isomerization product. The second model also contains the self-reaction of the isomerization product. Both models make use of Mollner's k_{isom}/k_{O2} value obtained before the reanalysis of the kinetics data;[30] however, we show in the next section that the exact value of k_{isom}/k_{O2} is irrelevant. By examining only these reactions, we can determine if the low [O_2] anomaly persists in the absence of secondary chemistry.

Table 9.10. First Reduced Kinetics Model for *n*-butoxy (primary reactions only)

A[a,b]	***Ea*/*R*** **(K)**	**Reaction**	**Source**
5.80E+02	0	C4H9O==>C3H7+HCHO	Atkinson[142]
3.20E+05	0	C4H9O==>HOC4H8	Mollner[30]
1.40E−14	0	C4H9O+O2==>C3H7CHO+HO2	Atkinson[142]
3.80E−11	0	C4H9O+NO==>C4H9ONO	IUPAC[118]
7.50E−12	0	HOC4H8+O2==>HOC4H8OO	IUPAC[118]

a) Units of *A* are cm^3 $molec^{-1}$ s^{-1} for bimolecular reactions, and s^{-1} for unimolecular reactions
b) Termolecular reactions have already been converted to the effective bimolecular rate constant: the listed rate constants are valid at 670 torr, 298 K only

Table 9.11. Second Reduced Kinetics Model for *n*-butoxy (includes HOR• dimerization)

A[a,b]	***Ea*/*R*** **(K)**	**reaction**	**source**
5.80E+02	0	C4H9O==>C3H7+HCHO	Atkinson[142]
3.20E+05	0	C4H9O==>HOC4H8	Mollner[30]
1.40E−14	0	C4H9O+O2==>C3H7CHO+HO2	Atkinson[142]
3.80E−11	0	C4H9O+NO==>C4H9ONO	IUPAC[118]
7.50E−12	0	HOC4H8+O2==>HOC4H8OO	IUPAC[118]
5.00E−11	0	HOC4H8+HOC4H8==>HOC8H16OH	NIST[117]

a) Units of *A* are cm^3 $molec^{-1}$ s^{-1} for bimolecular reactions, and s^{-1} for unimolecular reactions
b) Termolecular reactions have already been converted to the effective bimolecular rate constant: the listed rate constants are valid at 670 torr, 298 K only

Plots of A_0/A vs [O_2] were generated in the same manner as described in the *Results* section for the full kinetics model, shown in Figure 9.6. Figures 9.6a and 9.6b make use of the first reduced kinetics model (no self-reaction of HOR•), while Figures 9.6c and 9.6d make use of the second reduced kinetics model (includes self-reaction of HOR•). The full [O_2] range is shown in Figures 9.6a and 9.6c, and the [O_2] anomaly region shown in Figures 9.6b and 9.6d. Over the entire [O_2] range, the agreement between the two reduced kinetics models and Garland's CRDS data is quite good. Ignoring the [O_2] = 0 data points and assuming 10% uncertainty in A_0/A on each data point, the reduced chi-squared statistic (χ_v^2) is 0.73 for the first kinetics model, and 0.72 for the second kinetics model. The full kinetics model (Figure 9.4) had $\chi_v^2 = 0.80$ (including all data points), essentially the same χ_v^2 as the reduced model. This confirms that secondary chemistry effects are minimal across the full range of [O_2]. At low [O_2], we notice that inclusion of HOR• self-reaction affects the agreement between the kinetics models and the CRDS data. Both reduced kinetics models qualitatively fit the CRDS data, but the agreement between simulation and CRDS data is poorer in the first kinetics model, where HOR• self-reaction is not accounted for. Ignoring the [O_2] = 0 data points and assuming 10% uncertainty in A_0/A on each data point, the reduced chi-squared statistic (χ_v^2) is 0.41 for the first kinetics model, and 0.31 for the second kinetics model. The full kinetics model had $\chi_v^2 = 0.64$ (all data points used), in good agreement with the both of the reduced kinetics models. We conclude that the cause of the low [O_2] anomaly lies in the primary alkoxy chemistry, and is mostly due to the change in OH stretch intensity between HOR• and HOROO•.

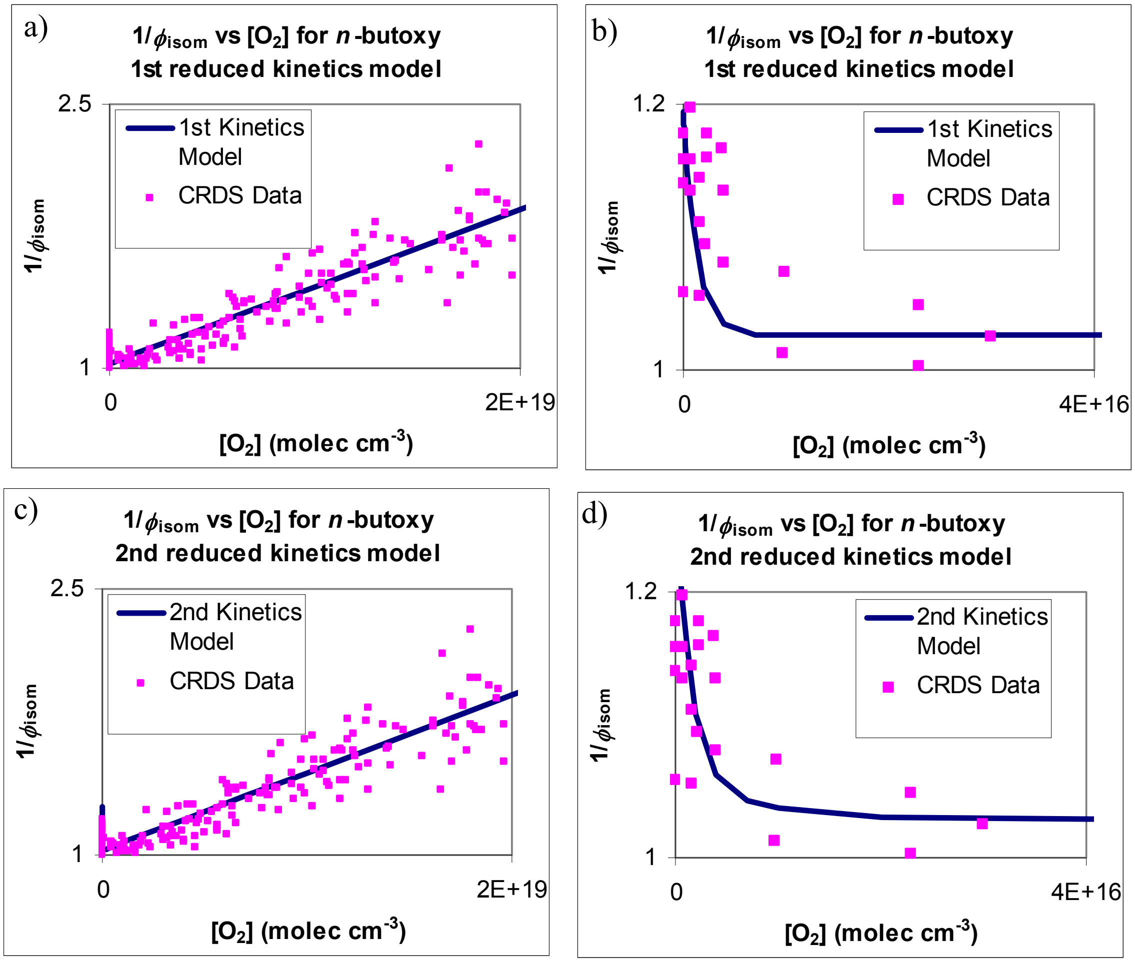

Figure 9.6 Comparison of A_0/A (labeled $1/\phi_{\text{isom}}$) vs [O_2] of *n*-butoxy for the reduced kinetics/quantum chemistry simulation (blue line) and our cavity ringdown study prior to reanalysis (pink squares), for [O_2] = $(0–2) \times 10^{19}$ molec cm^{-3} (a and c), and [O_2] = $(0–4) \times 10^{16}$ molec cm^{-3} (b and d). Parts a and b use a kinetics model that ignores self-reaction of HOR•, while parts c and d use a kinetics model including self-reaction of HOR•. The four plots show good agreement between the reduced kinetics model simulation and the CRDS data, indicating that most of the low [O_2] anomaly can be explained by the primary alkoxy chemistry, and thus the different OH stretch intensity of HOR• and HOROO•.

Persistence of Low [O_2] Anomaly for Other Values of k_{isom}/k_{O2}

The analysis of the low [O_2] anomaly up to this point has made exclusive use of our value for $k_{\text{isom}}/k_{\text{O2}}$ of 1.69×10^{19} cm^{-3}. However, the scatter in $k_{\text{isom}}/k_{\text{O2}}$ from previous experiments yields values over the range $(1–3) \times 10^{19}$ cm^{-3}. This raises the question of whether or not the low [O_2] anomaly will persist in our kinetics simulations for smaller values of $k_{\text{isom}}/k_{\text{O2}}$. Since $k_{\text{isom}}/k_{\text{O2}}$ is predicted to be temperature dependent,[129-140] such information will be useful for future spectroscopists.

To test this idea, we re-ran our full *n*-butoxy kinetics model using a different rate constant for the isomerization reaction. We chose to use one of the lowest value for the ratio of rate constants in Table 9.1 including uncertainty $k_{\text{isom}}/k_{\text{O2}} = 1.1 \times 10^{19}$ molec cm^{-3}.[156] To apply this new ratio to our kinetics model, we kept k_{O2} constant,[118] and changed the rate constant for isomerization from 3.2×10^5 s^{-1} to 1.5×10^5 s^{-1}. The rest of the kinetics model remained unchanged. We then generated new plots of A_0/A vs [O_2] as described above. Figure 9.7 compares the simulated A_0/A vs [O_2] for Cox's value of $k_{\text{isom}}/k_{\text{O2}}$ (1.1×10^{19} molec cm^{-3}, blue curve) to Mollner's value (2.3×10^{19} molec cm^{-3}, pink curve).

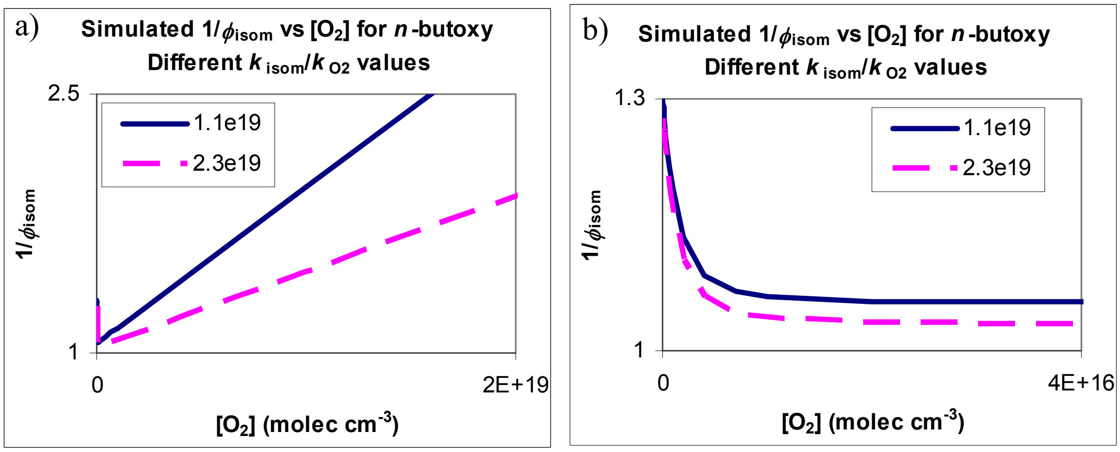

Figure 9.7. Comparison of simulated A_0/A vs [O_2] for *n*-butoxy, using two different values of $k_{\text{isom}}/k_{\text{O2}}$. The blue curve uses Cox's value of 1.1×10^{19} molec cm^{-3},[156] while the pink dashed curve uses Mollner's value of 2.3×10^{19} molec cm^{-3}.[30] The full range of [O_2], $(0–2) \times 10^{19}$ molec cm^{-3}, is shown in part a, while the [O_2] anomaly region, $(0–4) \times 10^{16}$ molec cm^{-3}) is shown in part b. Although the curves have different slopes and values in each region, we observe that the low [O_2] anomaly still appears at the reduced value of $k_{\text{isom}}/k_{\text{O2}}$.

In Figure 9.7a, we immediately notice a steeper slope for the $k_{\text{isom}}/k_{\text{O2}} = 1.1 \times 10^{19}$ molec cm^{-3} case, as predicted by Equation 9.8. Of greater interest to us is the curvature shown in Figure 9.7b. For both values of $k_{\text{isom}}/k_{\text{O2}}$, the apparent A_0/A decreases sharply as $[\text{O}_2]$ is increased to 10^{14} molec cm^{-3}, followed by a slow and steady decrease as $[\text{O}_2]$ is further increased to 4×10^{16} molec cm^{-3}. Although the specific values of A_0/A differ between the two simulations, the low $[\text{O}_2]$ anomaly still appears in the same $[\text{O}_2]$ region. This observation agrees with our idea that the change in OH stretch intensity between HOR• and HOROO• is the dominant cause of the low $[\text{O}_2]$ anomaly. Any future spectroscopic experiments should be able to observe the low $[\text{O}_2]$ anomaly, regardless of the specific value of $k_{\text{isom}}/k_{\text{O2}}$ that is measured. Because Figure 9.7b shows that the curvature is dependent on $k_{\text{isom}}/k_{\text{O2}}$, it may be possible to use the low $[\text{O}_2]$ region in rate constant fitting to obtain values of $k_{\text{isom}}/k_{\text{O2}}$ with lower uncertainties.

Conclusions

We have generated a combined chemical kinetics and quantum chemistry model to determine the products being detected in our alkoxy relative kinetics experiment, develop a general framework for the OH stretch absorption properties of ROH, HOR•, and HOROO• isomers, and explain the anomalous behavior of the ν_1 relative absorption A_0/A at low $[\text{O}_2]$. We have shown that after 110 μs, only 50%–80% of the products being detected are the primary products of isomerization HOR• or HOROO•, with the remainder belonging to stable end-products. By examining alkoxy systems of different chain lengths and functional group positions, we also show that the relative positions of the hydroxy group and radical center/peroxy group govern how the OH stretch position and intensity will change. We have shown that the anomalous behavior of A_0/A at low [O_2] can be explained solely due to the change in the OH stretch intensities of the products being detected (HOR• at low [O_2], HOROO• at high [O_2]). Our kinetics and quantum chemistry simulations produce A_0/A vs [O_2] plots in excellent agreement with the CRDS data presented in Chapter 8, indicating that our model fully captures the essential chemistry occurring in the alkoxy system. The low [O_2] anomaly occurs independently of the specific value of $k_{\text{isom}}/k_{\text{O2}}$ measured, indicating that general spectroscopic studies on the OH stretch of alkoxy products will exhibit the same anomaly.

Acknowledgements

The models developed in this chapter were funded under NASA Upper Atmosphere Research Program Grants NAG5-11657, NNG06GD88G, and NNX09AE21G2, California Air Resources Board Contract 03-333 and 07-730, and a Department of Defense National Defense Science and Engineering Graduate Fellowship (NDSEG).